REPORT DOCUMENTATION PAGE

Form Approved
OBM No. 0704-0188

1. AGENCY USE ONLY *(Leave blank)*	2. REPORT DATE	3. REPORT TYPE AND DATES COVERED
	December 1997	Contract Report

4. TITLE AND SUBTITLE

Final Report on Comparison of Drogued and Undrogued Drift Buoys

5. FUNDING NUMBERS

Job Order No.

Program Element No. 0603207N

Project No.

Task No.

Accession No.

6. AUTHOR(S)

Stephen E. Pazan

7. PERFORMING ORGANIZATION NAME(S) AND ADDRESS(ES)

Ocean Prospects
204 N. El Camino Real, Suite 619
Encinitas, CA 92024

8. PERFORMING ORGANIZATION REPORT NUMBER

NRL/CR/7401--98-0003

9. SPONSORING/MONITORING AGENCY NAME(S) AND ADDRESS(ES)

Naval Research Laboratory
Center for Tactical Oceanographic Warfare
Stennis Space Center, MS 39529-5004

10. SPONSORING/MONITORING AGENCY REPORT NUMBER

11. SUPPLEMENTARY NOTES

In support of Basic Contract No. N00014-95-C-6002

12a. DISTRIBUTION/AVAILABILITY STATEMENT

Approved for public release; distribution unlimited

12b. DISTRIBUTION CODE

13. ABSTRACT *(Maximum 200 words)*

This is the final report for a three year study to retrieve Lagrangian velocity estimates from comparisons of Naval AN/WSQ-6 (METOCEAN CMOD) drifting buoy observations and Tropical Ocean/Global Atmosphere (TOGA) and World Ocean Climate Experiment (WOCE) Lagrangian drifter observations in order to develop and improve the state-of-the-art in ocean current observations and upper ocean modeling products for Navy fleet use. Navy buoy drogues are relatively small and subject to surface currents and surface wind and wave forcing; consequently, the buoys deviate from the path of a Lagrangian drifter drogued at a depth of 15 m. After they lost their drogues, WOCE/TOGA buoys could be expected to have behaviour similar to Naval AN/WSQ-6 buoys. Because data has been available from WOCE/TOGA Lagrangian drifters deployed during the same period, and these drifters have been designed to move with the currents at 15 m depth, we can compute *deviant drift velocity* from near-simultaneous and co-located observations of the *observed drift velocity* by both Naval AN/WSQ-6 buoys and WOCE/TOGA buoys under many wind and wave conditions. The extent of this deviation varied with buoy design, wind strength, wave conditions and the vertical current shear. A test of a drag force model in the tropical Pacific has shown that the most significant deviant drift-producing forces in the least-square sense were due to winds or surface gravity waves, jointly accounting for 85% of the variance. Without wind and wave forcing and disregarding small effects due to mixing, a neutrally buoyant object move just as a water parcel of identical size and shape moved. The effect of wind and wave forcing is to accelerate the object relative to the water until forcing was balanced by fluid drag. The terminal velocity attained relative to the water, called *slip velocity*, depends upon the drag cross-section of a buoy or vessel relative to wind and waves. Every object slips but the slip of SVP WOCE buoys has been observed and was about 0.1% of the wind speed. This study examined the combined effects of slip and vertical current shear on the deviation

14. SUBJECT TERMS

drogued buoys, undrogued buoys, Lagranian estimates, AN/WSQ-6 buoys, FNMOC, WOCE, TOGA, and ECMWF

15. NUMBER OF PAGES

57

16. PRICE CODE

17. SECURITY CLASSIFICATION OF REPORT	18. SECURITY CLASSIFICATION OF THIS PAGE	19. SECURITY CLASSIFICATION OF ABSTRACT	20. LIMITATION OF ABSTRACT
Unclassified	Unclassified	Unclassified	SAR

THERE ARE NO PAGES MISSING

REPORT COMPLETE AS IS

PER: STEPHEN PAZAN

(760) 753-9328

OCEAN PROSPECTS

ENCINITAS, CA.

UNCLASSIFIED

Ocean Prospects Report 97-2

Final Report on Comparison of Drogued and Undrogued Drift Buoys

Stephen E. Pazan

Ocean Prospects
204 N. El Camino Real, Suite 619
Encinitas, CA 92024-2867

COTR: Harry Selsor (1994-1996); Edward Mozley (1997)
Naval Research Laboratory, Code 7406
Stennis Space Center, MS 39529-5004
Contract N00014-95-C-6002

Ocean Prospects
204 N. El Camino Real, Suite 619
Encinitas, CA 92024

ABSTRACT

This is the final report on a three year program to retrieve Lagrangian velocity estimates from observations of Naval AN/WSQ-6 drift buoys for the benefit of naval operations. Ocean Prospects has fulfilled the tasks specified in the contract, quality controlling wind and buoy data, making comparisons of drogued and undrogued buoy observations, and developing both 1-D and 2-D linear regression models of buoy drift. Ocean Prospects archived and quality controlled 1,844,144 drogued WOCE buoy observations, 848,416 undrogued WOCE buoy observations, and 196,885 Naval AN/WSQ-6 buoy observations at synoptic time intervals, as well as synoptic fields of FNMOC and ECMWF winds. Meridional and zonal surface wind velocity components from the global synoptic FNMOC model and the global synoptic ECMWF model were interpolated to each Naval AN/WSQ-6 and WOCE/TOGA buoy position and date/time in the datasets. Seven 1-D linear regression models were evaluated for both the Navy vs. WOCE drogue-on dataset and the WOCE drogue-off vs. WOCE drogue-on dataset. Principal results from this analysis were: the constant term in the regression analysis was zero; both the regression coefficients and variance explained were the same within error for regressions using Navy buoy velocity or undrogued WOCE buoy velocity as dependent or predictor variables, i.e. the Navy buoys behaved like undrogued WOCE buoys; the regression coefficients and variance explained were the same within errors for either FNMOC or ECMWF winds and for the purposes of this study, either FNMOC or ECMWF winds were sufficient. The 2-D regression analysis on selected synoptic data was:

$$U_{undrogued} - U_{drogued} = B \cdot W,$$

where U was buoy drift velocity (cm/sec) and W is wind velocity (m/s); the real and imaginary parst of these quantities were the zonal and meridional components, respectively. B was the complex valued regression coefficient; the constant term was constrained to be zero as a consequence of the results of the 1-D analysis. We found that the absolute value of B was a function of the reciprocal of the square root of the Coriolis parameter, f, 1.458×10^{-4}(sec^{-1}), giving:

$$|B| = (B_0 + B_1 \cdot f^{-1/2}),$$

where the best fit gives B_0=-0.257 (cm/m), and B_1=1.305 (cm/m sec$^{1/2}$). These results were confirmed by analyses of binned mean buoy drift on binned mean wind. A dataset assembled from undrogued (Navy) and drogued buoy pairs was analyzed and results confirm the amplitude of the mean coefficient. The bin analysis also found that the angle of response, θ, was a function of the surface wind and the Coriolis parameter:

$$\theta = Phase(B) = (\theta_0 + \theta_1 \cdot |W| \cdot f^{-1/2}),$$

where θ ranged from 20° to 35° to the left (right) of the wind north (south) of the equator from 20° to 50° in latitude; it is best fit by θ_0 =14.9° and θ_1 = 0.75 (degrees sec$^{1/2}$/m). A corrected Navy buoy and WOCE drogue-off dataset has been created and is available from Ocean Prospects.

Contents

Acknowledgements

I would like to acknowledge first the contributions of Prof. Peter Niiler, whose advice and assistance has been essential to this project from inception to completion. Harry Selsor, the COTR for this contract, deserves thanks for his constant encouragement and help. Mrs. Frances Bang, his secretary, has helped countless times to smooth communications over half a continent. Ray Mahr, METOCEAN's representative at NRL SSC has always been ready to answer questions about the Navy CMOD buoy which his company manufactures. Thanks to Harley Hurlburt, Charlie Barron Joseph Metzger, Steve Piacsek and Alex Warn-Varnas for informative discussions. Thanks to Andre Bolduc (MEDS), Dennis Laws (FNMOC), and Roy Lowry (Bidston UK) for their help with data issues. Thanks to Andy Sybrandy, Elise Ralph, Sharon Lukas and Judy Gauke of SIO for their help with the WOCE/TOGA dataset.

1. Introduction

This is the final report for a three year study to retrieve Lagrangian velocity estimates from comparisons of Naval AN/WSQ-6 (METOCEAN CMOD) drifting buoy[1] observations and Tropical Ocean/Global Atmosphere (TOGA) and World Ocean Climate Experiment (WOCE) Lagrangian drifter observations in order to develop and improve the state-of-the-art in ocean current observations and upper ocean modeling products for Navy fleet use. Navy buoy drogues are relatively small and subject to surface currents and surface wind and wave forcing; consequently, the buoys deviate from the path of a Lagrangian drifter drogued at a depth of 15 m. After they lost their drogues, WOCE/TOGA buoys could be expected to have behaviour similar to Naval AN/WSQ-6 buoys. Because data has been available from WOCE/TOGA Lagrangian drifters deployed during the same period, and these drifters have been designed to move with the currents at 15 m depth, we can compute *deviant drift velocity* from near-simultaneous and co-located observations of the *observed drift velocity* by both Naval AN/WSQ-6 buoys and WOCE/TOGA buoys under many wind and wave conditions. The extent of this deviation varied with buoy design, wind strength, wave conditions and the vertical current shear. A test of a drag force model in the tropical Pacific has shown that the most significant deviant drift-producing forces in the least-square sense were due to winds or surface gravity waves, jointly accounting for 84% of the variance (Niiler *et al.*, 1987; Niiler *et al.*, 1995). Without wind and wave forcing and disregarding small effects due to mixing, a neutrally buoyant object move just as a water parcel of identical size and shape moved. The effect of wind and wave forcing is to accelerate the object relative to the water until the forcing was balanced by fluid drag. The terminal velocity attained relative to the water, called *slip velocity,* depends upon the drag cross-section of a buoy or vessel relative to wind and waves. Every object slips but the slip of SVP WOCE buoys has been observed and was about 0.1% of the wind speed (Niiler, *et al.*, 1995). This study examined the combined effects of slip and vertical current shear on the deviation of undrogued/Navy buoys drift from the drift of a drogued buoy. The relationship of vector wind, slip and buoy drift is graphically illustrated in **Figure 1**. The *drift deviation* which has been the subject of this study differed from the problem of *slip* because of the inclusion of vertical current shear between 15 m depth and the surface; it is like the problem of *slip* in that the difference between buoy drift drogued at 15 m depth and the surface drift of undrogued buoys was also a function of the wind and wave conditions. Therefore, although analysis of undrogued/Navy buoy deviant drift, U_D, has lent itself to a better understanding of *slip*, U_s, it didn't solve the separate problem of *slip*. The present study has developed a parameterized model of the deviant drift. Once having modeled *deviant drift*, we subtracted *deviant drift* from the *observed surface drift velocity* , U_u, and obtained the true *upper ocean drift, U_{15}, that drift which would be observed by a buoy drogued at 15 m.* This was done, creating the Auxiliary Lagrangian Drifter Dataset (ALDD). consisting of synthetic Lagrangian drift velocities and error estimates that can be assimilated into oceanographic models.

As explained in the first annual report, synthetic Lagrangian drift velocities increase the usefulness of Naval AN/WSQ-6 buoys to Navy operations, FNMOC ocean modeling, climate forecasting, and oceanographic research, objectives endorsed by Section 7410 of the NRL BAA 94-1. Benefits not only accrue from a better quality of the buoy data, but also from understanding the error and reliability of these data, according to FNMOC at Monterey. There will be a great increase in usable drift buoy data in the Indian Ocean and western tropical Pacific which will complement and usefully supplement the drift buoy data presently available for the WOCE/TOGA programs and oceanographic research in general.

Wind and buoy data was acquired, quality controlled, and drogued buoys compared with undrogued buoys in order to select times and areas for modelling deviant drift and retrieving Lagrangian drift vectors. The quality control of Fleet Numerical Meteorology and Oceanography Central (FNMOC) wind data was more extensive than previous experience would have predicted and occupied considerable effort. Because of uncertainties with the FNMOC wind fields, wind data from the European Medium-Range Weather Forecasting (ECMWF) Center was also acquired and compared with the FNMOC wind data, and both were used in development of a statistical model of drifter response to wind forcing. Once

[1] The manufacturer's designation is "*Compact Meteorological and Oceanographic Drifter*"; the Navy has also designated this buoy the "*Combat Meteorological and Oceanographic Drifter,*" (Selsor, 1993).

encoding and decoding errors were rectified, FNMOC winds performed as well as ECMWF winds and the final Auxiliary Lagrangian Drifter Dataset was created using FNMOC winds.

2. Data and Procedures

2.1 Naval AN/WSQ-6 Drifter Data

Details of the Navy buoys are described in Appendix A. Data from Naval AN/WSQ-6 buoys deployed since 1990 have been obtained from the Canadian Marine Environmental Data Service (MEDS), which acted as the data distribution center for the WOCE/TOGA Surface Velocity Program (SVP). However, this data was not archived as a separate dataset at MEDS and it was necessary to specify the ARGOS identification numbers to the MEDS staff in order to selectively obtain it. ARGOS buoy numbers were obtained from the Oceanographic Processing branch of NDBO and forwarded to MEDS, which extracted the data for all buoys with the specified identifications between the years January 1, 1990 and December 31, 1994; since the data was obtained in 1995, the MEDS dataset was incomplete for the last half of 1994.

During the five years since 1989, 706 METOCEAN Naval AN/WSQ-6 buoys were deployed in the Atlantic, Pacific and Indian Ocean; these buoys returned 334,944 buoy observations at time intervals determined by ARGOS satellite reception times. Global monthly summaries of the Naval AN/WSQ-6 Navy drift buoy dataset are shown in **Figure 2,** and the global distribution of Naval AN/WSQ-6 drift buoy data is displayed in **Figure 3 (top).** Data from 704 Navy buoys have been interpolated to 196,885 synoptic 4-daily time intervals for consistency with both WOCE/TOGA datasets; the interpolated dataset has buoy observations at 4-daily synoptic time intervals. A linear interpolation to synoptic times was used (see section 2.5, below). Ocean Prospects received these data from MEDS in General Format 3 (GF-3) format. A brief overview of the GF-3 software is in Appendix B.

2.2 WOCE/TOGA Lagrangian Drifter Data

The World Ocean Circulation Experiment (WOCE) and Tropical Ocean and Global Atmosphere (TOGA) projects have deployed 2013 WOCE/TOGA Lagrangian drifters during 1990-1994. We archived these data and data from 1632 WOCE/TOGA drifting buoys after they lost their drogues, a dataset comprising 1,844,144 drogued buoy observations and 848,416 undrogued buoy observations at synoptic time intervals; the quality control of these data has been described in Poulain and Hansen (1996). Global monthly summaries of the WOCE/TOGA Lagrangian drifting buoy dataset are shown in **Figure 2.** The global spatial distribution of WOCE/TOGA drogued and undrogued drift buoy data for the years 1990 through 1994 is displayed in **Figure 3 (middle and bottom).**

Each of the TOGA/WOCE Lagrangian drifters had a drogue on/drogue off sensor that determined whether the spherical surface float was out of water or underwater. So long as the drogue is attached, the surface float tended to submerge; if the surface float is continuously out of the water, the buoy was assumed to have lost its drogue. As explained below, in 400 days of deployment about half of the WOCE buoys will have lost their drogues, consistent with previous findings (Sombardier & Niiler, 1994), although this might have been shorter in harsher environments (Poulain *et al.*, 1996), and after accounting for buoys which become inoperative due to other causes. The decline in drogued buoy population was highly variable; the decay was not exponential nor is it clearly linear. It can be said that it was consistent with a "noisy" linear decline, implying that a fixed number of buoys, not a fixed proportion of buoys, lose their drogues in any time interval; this was equivalent to the probability of drogue failure increasing with time. Niiler and Sybrandy (private communication) have found from six recovered drifters in the tropical Pacific of the same design and manufacture as those study herein that the tether connecting the buoy with its drogue was bitten by fish and appeared to sever just above the subsurface float carrot.

2.3 Wind and Wave Data

FNMOC produces marine synoptic six-hourly wind and wave analyses on a global grid; ECMWF produces marine synoptic 12-hourly wind analyses, also on a global grid. Since the buoy data positions either are archived at synoptic six-hourly intervals or interpolated to synoptic six-hourly intervals, we interpolated synoptic wind and wave values to the location of individual buoy observations from the four surrounding FNMOC or ECMWF grid field values. Wind or wave data were also interpolated in time when data were

missing at any particular synoptic time or at every 06 GMT and 18 GMT synoptic time, in the case of ECMWF data.

2.4 Statistical Summaries

We have made statistical summaries of buoy drift velocity, ECMWF and FNMOC wind velocity and FNMOC wave height in 2° latitude × 8° longitude × 1 month bins. Binning removed random variance through averaging, and therefore revealed underlying relationships which might otherwise be obscured by noise. Because these statistical summaries included standard deviations as well as mean quantities, they were used to remove bias in the regression and estimate confidence limits. The summaries were of two kinds: first, separate drogued and undrogued (Navy) statistics were computed of all quantities associated with selected buoys; second, combined statistics were computed of all quantities associated with selected pairs of drogued and undrogued (Navy) buoys. The distribution of the first type of summary bins was roughly equivalent to the distribution of observations shown in **Figure 3**. The second type of summary had a more restricted distribution; there were about 3001 of these bins in the WOCE On/Off buoy pair dataset, and about 565 of these bins in the WOCE On/Navy buoy pair dataset; eliminating null and suspect values reduced the numbers of bins actually used in the analyses. The geographical distribution of these buoy-pair bins is mapped in **Figure 21 (top).**

2.5 Regional Selection

There were three important considerations in the selection of potential study areas: 1. the buoys to be intercompared should have been close enough to be in the same ocean current; 2. the ocean region should have been one of low vertical and horizontal shear; 3. the ocean region should have relatively steady wind velocity and wave energy. These considerations generally excluded use of data from boundary currents or equatorial currents. As shown in **Figure 3** TOGA/WOCE drifters hin 1990-1994 were deployed extensively in the Atlantic and Pacific, from the tropics to the Arctic. The trade wind regions were favorable to this study because of the relatively large decorrelation scales and low vertical and horizontal shear. In **Figure 5** four selected regions of relatively low wind speed variability and wave height variability have been outlined (see also table I) and displayed. Climatological horizontal shear in the upper ocean was low and observational density was relatively high in this regions, with the exception of the equatorial Pacific, which was chosen to provide some insight into processes near the equator.

TABLE I. Bounds of selected regions.

REGION	SOUTH	NORTH	WEST	EAST
	LATITUDE		LONGITUDE	
EASTERN N. PACIFIC	10°N	50°N	160°E	120°W
EASTERN S. PACIFIC	35°S	10°S	150°W	80°W
EASTERN N. ATLANTIC	10°N	50°N	50°W	10°W
EQUATORIAL	10°S	10°N	100°E	0°

3. Quality Control

3.1 Source Institution Quality Control

Quality control procedures developed by the Buoy Data Center at AOML have already examined the WOCE/TOGA data records for internal consistency, positioning errors and outliers. We did find occasional inconsistencies between this record and the buoy metafile describing the WOCE/TOGA drifting buoys, which were reported to members of Professor Niiler's research group at the Scripps Institution of Oceanography who, at the time, were given responsibility for management of the WOCE/TOGA metafile data base and the WOCE/TOGA drift buoy dataset, respectively. Appropriate action was taken in each case. MEDS has done similar internal consistency, and positioning error checks in the Navy buoy dataset, but there were problems in the Navy dataset which did not occur in the WOCE/TOGA dataset. Sometimes positions do not change from one observation to the next and at the end of a record there were often several observations from a single position. We considered these cases of the terminal doldrums to be specious and did not include them in the analysis. This has required examining each record, which occasionally has revealed large shifts in position within a few hours, something which should have been caught by a positioning error check. Sometimes the day and month changed from December 31 to January 1 but the year didn't. The only identifiers for these records which

MEDS appended were the ARGOS identification numbers. These were wholly insufficient, as new buoys were given the old ARGOS id after it was retired. Fortunately, it was almost always easy to determine where a new buoy was deployed because of the large time and space interval which occured between the last observation of one deployment and the first observation of the next deployment.

3.2 Wind Dataset Quality Control

We found occasional inconsistencies within the FNMOC wind and wave dataset. The FNMOC winds sometimes had the incorrect century, but this was trivial to correct. There have been other formatting errors, inconsistent with the official GRIB system (Appendix C), which did not affect the data and were easy to account for. The FNMOC wind format was inadequately documented and changed between 1992 and 1993; the longitude and latitude axes were swapped between 1991 and 1992; and the longitude origin was displaced from the prime meridian by different amounts before and after 1992. There were also several GRIB encoding errors. After solving these problems, the FNMOC and ECMWF wind fields compared well. Scatterplots of interpolated FNMOC winds vs. interpolated ECMWF winds were made for the WOCE/TOGA drogue-on/drogue-off dataset (hereinafter called "WOCE On/Off Dataset") and the WOCE/TOGA drogue-on/Navy dataset (hereinafter called "WOCE On/Navy Dataset") and are shown in **Figure 4 (bottom)** and **Figure 4 (top)**, respectively. Correlations of FNMOC and ECMWF fields were tabulated in Table I.

TABLE I. ECMWF-FNMOC CORRELATION

	ZONAL	MERIDIONAL
DROGUE OFF	95.7%	88.7%
NAVY BUOY	95.8%	94.3%

There are outliers by several standard deviations or more in each of these scatterplots which needed to be elided from the final analysis; comparison of the wind datasets provides an extra quality control check on the wind data.

3.3 Linear Interpolation

Navy AN/WSQ-6 buoys had to be interpolated to synoptic time intervals for consistency with WOCE/TOGA data and FNMOC or ECMWF wind data. The linear interpolation (Appendix D) filtered buoy drift variability at time scales shorter than the interval between observations. The effect has been to smooth out sub-synoptic scale variability, which is an advantage since this study focused on time scales greater than two days, which was eight six-hourly synoptic periods. In consequence of this, I have used this method to interpolate all of the Navy buoy data to synoptic intervals.

4. Buoy Survivability

4.1. Introduction

As stated above, each of the TOGA/WOCE Lagrangian drifters has a drogue on/drogue off sensor that determined whether the spherical surface float was out of water or underwater. Since inoperability due to drogue loss or transmitter failure was a failure of the drift buoy system, and other major causes of inoperability such as theft and running aground cannot be called system failures, drogue loss and transmitter failure were considered the most important measures of drift buoy survivability by the scientific community. Therefore, the first measure of survivability of these drifters has been taken to mean "survivability against drogue loss." Since the Naval AN/WSQ-6 buoys operated without a drogue on/drogue off sensor, and since the drogue was relatively much smaller anyway (see **Figure A.1** and **Figure A.2**), their survivability has been defined as survivability against transmitter failure; these buoys could lose their drogues, continue to return data, and still be considered operable. In order to measure survivability and compare survivability of Lagrangian drift buoys and Naval AN/WSQ-6 buoys, we made three separate assessments: 1. WOCE/TOGA drift buoy survivability to drogue loss; 2. WOCE/TOGA drift buoy survivability to all other forms of failure (principally transmitter failure); 3. Naval AN/WSQ-6 buoy survivability to to all other forms of failure.

I. 4.2 Drogue Loss

It was important to examine drogue loss in order to make improvements in survivability. Drogue loss was susceptible to an engineering fix and that alone made drogue loss more interesting than most other failure modes.

In order to obtain an accurate predictor of drogue

loss it wa necessary to normalize the surviving buoy population, not to the total population of buoys, but only to that sub-population which survived with or without drogues for that duration, because only that part of the population had the opportunity to lose a drogue, either in the past or in the future. Therefore, for any particular survival duration, buoys which had been deployed too recently to have had the possibility of surviving for that duration or buoys which grounded, were stolen, or had electronics failure before surviving that long were not included in the drogue survivability estimate.

We wish to find the drogue losses N_d at time t=T of N_0 buoys deployed at time t=0. We only assume that the same percentage of buoys will have lost their drogues by time T no matter how many buoys have been deployed at time 0. This gives the governing equation:

$$N_d(T) = P_d(T) \cdot N_0. \qquad (1)$$

where $P_d(T)$ is the proportion of buoys which have lost their drogues at time t=0; the failure rate $R_d(t)$, is related to $P_d(T)$ by the equation:

$$P_d(T) = 1 - \int_0^T R_d(t)\, dt\,. \qquad (2)$$

However, drogue loss was not the only mode of failure, as already explained (above); if we make the same assumptions about these other modes of failure, at time T a proportion Q(T) of these buoys will have failed through one of these other failure modes:

$$N_q(T) = Q(T) \cdot N_0. \qquad (3)$$

Assuming that drogue loss and these failure modes are independent, it follows that,

$$N_d(T) = P_d(T) \cdot Q(T) \cdot N_0. \qquad (4)$$

and

$$P_d(T) = N_d(T)/(Q(T) \cdot N_0). \qquad (5$$

I have computed $P_d(T)$ for observed times and plotted it for the WOCE drift buoys in **Figure 6**. The results indicated a buoy half-life of over 400 days, consistent with previous findings (Sombardier & Niiler, 1994). The decline in drogued buoy population was linear (or quadratic), as if a fixed (linearly increasing) number of buoys, not a fixed proportion of buoys, lost their drogues in any time interval. The lack of a proportional failure rate implied that the particular mode of this failure is not intrinsic to the buoy itself since most conceivable engineering/design failures would either have a constant or increasing probability of occurrence, giving an exponentially decaying population, not a linearly decaying population. A failure mode which depended upon some extrinsic feature of the buoy population, such as the number of buoys per unit area, could produce a linearly decaying population[2]. One possible extrinsic class of failure modes is predation. Niiler and Sybrandy found that the tether connecting the buoy with its drogue is severed at its weakest link by fish predation. The fish bites are random along the tether line, and if one occurs at the critical point above the subsurface float, drogue loss will rapidly follow. Thus the model of a constant number of bites per fixed length of drogue line would yield a model of a constant decay rate.

4.3 Other Modes of Failure

Other modes of failure often have intrinsic causes, such as electronics or power failure. The probability of failure due to all other causes can be taken to be constant at any time. This was confirmed by comparing a simple model based upon this assumption with the observed drifting buoy survivability. We have developed this simple model as follows: since any buoy in the population of drifting buoys, N_q (ref. equation 3), had a constant probability of failing, p, in a fixed time interval, Δt, on average the population of drifting buoys decreased by pN_q in the time Δt. This gives a governing equation:

$$\partial N_q/\partial t = -p \cdot N_q. \qquad (6)$$

[2] Here we have reversed the usual nomenclature used in thermodynamics, where the state of a system may depend upon intrinsic quantities, such as temperature, or extrinsic quantities, such as heat.

After integrating over time t from 0 to T, we find:

$$\ln(N_q) - \ln(N_0) = -p \cdot T. \qquad (7)$$

The number of surviving drift buoys declines linearly as function of time if plotted on a log-normal graph.

The inverse of the probability of failure per unit time, p_q, also called the e-folding period is the time it takes the population to reduce to 1/e of its original size. The conventional decay time is usually taken to be the half-life, which is inversely proportional to the probability of failure; the half-life is given by $\ln(2)/p_q$. In order to validate the exponential model for Navy buoys as well as WOCE/TOGA Lagrangian drift buoys, the natural log of the buoy populations, $\ln(N_q)$, versus the duration of deployment, T, and the linear regression of $\ln(N_q)$ on T is displayed in **Figure 7** and **Figure 8** for the WOCE/TOGA Lagrangian drift buoys and the Naval AN/WSQ-6 buoys, respectively. The equation of the least-squares linear regression is printed on each figure, as well as the e-folding period, the half-life, and R^2, the variance of the buoy population, N_q, normalized by the variance of the linear regression (if the linear regression explains all the variance, $R^2 = 1$). $R^2 = 0.995$ for Pacific WOCE/TOGA Lagrangian drifting buoys (**Figure 7**), indicating a very good fit to a model based on the assumption that failure is random and the probability of failure is a constant. The fit is also good for Atlantic WOCE/TOGA Lagrangian drifting buoys, which have an $R^2 = .939$. The Navy buoy population also fits this model since $R^2 = .988$ (**Figure 8**). The half-life of the WOCE/TOGA Lagrangian drifting buoys is between 161 (Atlantic) and 198 (Pacific) days; it must be emphasized here that this "lifetime" is a different quantity than the drogue failure lifetime discussed in section 4.2. The observed half-life of the Navy buoy population is 54 days and the exponential model half-life is 39 days. The model probability of any WOCE/TOGA Lagrangian drifting buoy failing during a given day is between 1/232 (Atlantic) and 1/285 (Pacific), whereas the model probability of a Navy buoy failing during a given day is 1/56. The observed probability of failure differs from the average probability of failure to the extent that the exponential model failed to correctly predict buoy survivability, a measure of which was the deviation of the observed buoy population from the exponential model. I have explored this for the Navy buoys by plotting the observed deviation for each of the years 1990, 1991, 1992, 1993, and 1994 in **Figure 9.** Survivability seemed to deviate from the regression equation in a systematic fashion; the plotted residuals look like a damped oscillator. The number of surviving buoys always seemed to start lower than would be predicted by the exponential model; then after 50 to 100 days, the number exceeded the prediction of the exponential model, followed by an increasing failure rate. This means that the failure rate was lower than normal until about 50 days after deployment; this may be because a particular failure mode became important after 50 to 100 days. If this failure mode can be identified and ameliorated it would be possible to increase the survivability half life; a 78 day "potential" half-life was estimated by extrapolating the initial failure rate; the extrapolation is shown in **Figure 8**. Similar extrapolations for WOCE/TOGA buoy survivability estimated "potential" half-lives of between 363 and 446 days. "Potential" half-life is based on poorly understood processes and caution must be taken against too much being made of the possibility of extending buoy lifetime from these estimates. This figure also implied that the survivability of the Navy buoys has not systematically changed in the period 1990-1994.

5. Error Budget

5.1 Random Walk Dispersion

The movement of buoys deployed in clusters at the same time and place was a sum of mean displacement and horizontal diffusion. Eddy diffusion increased the mean separation distance between buoys with time. A dimensional argument based upon the linear diffusion equation implied that mean separation should increase as the square root of time; if the dispersion area of the buoys is taken to be proportional to the square of the mean separation, a linear regression explains about 51% of the variance in observed dispersion area in the WOCE/TOGA drogued Lagrangian drift buoy dataset. The conclusion is that the paths of two collocated buoys should deviate from one another over time; this places a limit on how well the drogued buoy-undrogued buoy drift deviation can be measured.

5.2 Structure Functions

Estimates of the error variance which we have made have usually been based upon the variance of binned observations, which is not

identical to the error variance; part of the variance of buoy drift from binned observations was correlated with the wind variance of course, and was best left out of the error budget. In order to better estimate the error of observations of Navy buoy position, WOCE buoy position, and wind velocity, I have estimated structure functions by differencing, squaring and summing pairs of these observed parameter values Following standard methodology, I assumed that observations of buoy drift ($\mathbf{u}_i$) and wind ($\mathbf{w}_i$) can be represented as a sum of the unobservable actual values of the variables (ξ, η) and a random error:

$$w_i = \xi_i + \delta_i$$
$$u_i = \eta_i + \varepsilon_i = \beta \cdot \xi_i + \varepsilon_i \quad (8)$$

Here β is the regression coefficient whose estimation was largely the objective of this study. The random errors, δ and ε, in wind and buoy drift respectively have been estimated by comparing observation pairs with a decreasing range of separations. As the separations decreased, the variance of the difference between observations of wind velocity and buoy drift decreased as well; as an example, **Figure 10** displays the variance of buoy drift as a function of separation. If there were no noise in the observation, as the separation decreased to zero, the variance would asymptotically approach zero as well. However, since there is noise, the variance asymptotically approaches a value which may depend upon latitude and longitude; these results are tabulated in **Table E-I, Table E-II, Table E-III, and Table E-IV** in **Appendix E.** Compensatory statistical techniques[3] were applied to the buoy-pair regression analysis. In this analysis, I have used these estimates of noise to unbiąs regression coefficient estimates in the buoy-pair analysis discussed in Section 6.7.

[3] First, in the regressions themselves, a ceiling is placed upon the acceptable buoy pair wind differences; I have used 1 m/s. Because the error analysis demonstrated that error variance decreases significantly as buoy separation is decreased at least to 50 km, we have selected buoy pair observations which are within 50 km of each other. We have also used a well-known statistical technique called the Berkson controlled variable model, in which the values of the measured predictor are 'set' to pre-selected fixed values, in this case integral values of the wind velocity. After this, the error in buoy drift can be taken care of by standard techniques, notably the use of weighted least squares regression.

6. Models of Drift Deviation

6.1 One-dimensional Models

In order to connect the results of this study with those of earlier studies, and to test certain statistical assumptions, a one-dimensional linear regression model following Poulain *et al.* (1996) has been used to determine $\mathbf{U}_{off}$, the velocity (cm/sec) of the buoy without a drogue (or Navy buoy with small drogue), in terms of $\mathbf{U}_{on}$, the velocity (cm/sec) of the buoy with a drogue, and **W**, the wind velocity (m/sec). Other models explored other interdependencies of $\mathbf{U}_{off}$, $\mathbf{U}_{on}$, and **W**. Altogether seven linear regression models were evaluated:

Model 1. $U_{off} = A + C \cdot U_{on} - B \cdot W$

Model 2. $U_{on} = A + C \cdot U_{off} + B \cdot W$

Model 3. $U_{off} = A + C \cdot U_{on}$

Model 4. $U_{on} = A + C \cdot U_{off}$

Model 5. $U_{off} = A + B \cdot W$

Model 6. $U_{on} = A + B \cdot W$

Model 7. $U_{off} - U_{on} = A + B \cdot W$

The **A** (cm/sec), **C** (cm/m•sec) and **B** (cm/m) coefficients were chosen to minimize the calculated residual variance estimates,

$$\varepsilon^2 = (y - A - C \cdot U - B \cdot W)^2, \quad (9)$$

where **y** is the dependent variable and U is the buoy drift velocity predictor variable, W is the wind velocity predictor variable, and ε is the observed residual from the model estimate. Poulain (1994) forced **A** =0, but I have chosen to test this assumption and have let **A** vary. The residual variance is a measure of the error only if the following three assumptions are true:

- ◇ A linear relationship exists between dependent variables and predictor variables in the underlying population;
- ◇ True residuals, ε, follow a Normal distribution with mean zero;

◇ True residuals, ε, have the same variance for all values of the predictors;

The regression models have been evaluated for both the WOCE On/Navy Dataset and the WOCE On/Off Dataset. The first assumption can be tested by examining scatterplots of buoy drift vs. wind; examples of such scatterplots are shown in **Figure 12 (bottom left)** for the WOCE On/Off Dataset and in **Figure 12 (bottom right)** for the WOCE On/Navy Dataset; these are scatterplots drawn from nearly the entire dataset and are very noisy as a consequence. The relationship is clearer in a scatterplot of binned mean deviant drift vs. wind speed shown in **Figure 18**, which is drawn from selected data. These results support the use of the 1st assumption. A test of the second regression analysis assumption is shown in **Figure 12 (top),** in which residuals from a 1-D model are plotted against observed wind speed. The largest residuals in the scatterplots are gray shaded. The scatterplots suggest an underlying linear trend but are noisy; the noise may have been due to spatial and time aliasing because binning was done over large space and time scales or because the relationship between drift and wind forcing varied geographically. The latter was true and will be examined in a later section. The shading in this figure is linked to that in **Figure 11**; the gray-shaded residual outliers occupied areas in the Kuroshio, the Kuroshio Extension, the North Equatorial Current and the Gulf Stream, all areas of high shear which we predicted might prove difficult to model. In **Figure 11 (right)** residuals have been plotted against the so-called "normal score."[4] Residuals drawn from a Gaussian Normal population will describe a straight line if plotted against the "normal score"; this is not true of any other distribution. For instance, residuals drawn from a population with a Poisson distribution will be concave upward, with a monotonically increasing slope, and residuals drawn from bimodal population will be divided into two straight lines joined at a cusp. **Figure 11 (bottom right)** for the WOCE On/Navy Dataset looks very much like a bimodal distribution, but **Figure 11 (top right)** for the WOCE On/Off Dataset is clearly not Normally distributed. The "normal score" plots confirm that drift in high-shear areas was statistically distinct from that in low-shear areas, and that a population drawn from low-shear geographic areas may have satisfied the regression assumptions even if a global population didn't. In a test of the third assumption, residuals were plotted against predicted drift in **Figure 12 (top right)** for the WOCE On/Navy Dataset and in **Figure 12 (top left)** for the WOCE On/Off Dataset. The third assumption would be violated if there were a distinct increasing or decreasing trend in these figures. The black shaded, or "low-shear" population had a flat trend, but no trend can be discerned in the extreme outliers of the gray-shaded, or "high-shear" population. The conclusion is that the regression error analysis applied best with a selected sub-population of either dataset and operational models of buoy drift should take geographical restrictions into account. With this caveat in mind the results of the global models will be examined below.

Results from an earlier study which was confined to the North Atlantic can be compared with results from this study; this earlier regression (Poulain, 1994; Poulain et al., 1996) assumed the constant term was equal to 0 and was done for the period 1 August, 1991-31 December 1993 in the area 15°W-20°E, 60°N-74°N. The buoy drift velocity dataset was drawn from 461 pairs of six-hourly krigged drogued and undrogued drifter observations; the regression of these velocities was done upon UK Meteorological Officesix-hourly wind products. The results are tabulated:

◇ Model 1: $U_{off}=0.84\pm0.04\ U_{on} + 1.05\pm0.07\ W_x$, $R^2=67\%$
$V_{off}=0.58\pm0.05\ V_{on} + 1.19\pm0.08\ W_y$, $R^2=54\%$

◇ Model 2: $U_{on}=0.59\pm0.03\ U_{off} - 0.39\pm0.07\ W_x$, $R^2=53\%$
$V_{on}=0.43\pm0.03\ V_{off} - 0.20\pm0.08\ W_y$, $R^2=30\%$

The statistic R^2, also called the "coefficient of determination," is an overall measure of the success of the regression in predicting the dependent variable from the predictors. The tabulated error is the standard deviation of the sampling distribution (also called the standard error) of the respective coefficient; 95% confidence limits for Poulain's results were calculated by using his tabulated standard deviations and assuming 459 degrees of freedom, two less than the number of observations in his dataset. Imagine drawing a population of subsamples of the observations and computing least-squares linear regressions upon these

[4] The normal score is calculated as follows: sort the residual values in ascending order and assign each value an index according to the sorted order. Sort and index a Normal population of the same size and with mean 0 and standard deviation of 1 in the same way. The normal score of each residual value is the deviation from the mean of that member of the Normal population with the same index as the residual value.

subsamples, thereby obtaining a population of regression coefficients. The tabulated coefficient error is a best estimate of the standard deviation of these coefficients. These coefficients and the variance explained have been compared with regression coefficients which have been calculated for the regressions of synoptic six-hourly WOCE/TOGA drogued buoy drift and Navy buoy drift on wind velocity and themselves for the period 1 January, 1990-31 December 1994. The regressions were done upon FNMOC or ECMWF six-hourly wind products and the buoy drift velocity dataset was drawn from 565 pairs of 2° latitude × 8° longitude binned synoptic six-hourly WOCE/TOGA drogued buoy and Navy buoy observations. The median number of observations in a bin was 66 and the maximum was 394; bin averages were over all time:

◇ Model 1: U_{off}=-0.45±1.21+ 0.41±0.05U_{on} +2.40±0.25W_x,
R^2=41% df= 330 s=0.21
V_{off}= 0.57±0.91 + 0.22±0.06V_{on} + 1.09±0.28W_y,
R^2= 7% df= 356 s=1.7

◇ Model 2: U_{on}= 4.56±0.05 + 0.46±0.05U_{off} - 0.09±0.30W_x,
R^2=24% df= 330 s=23
V_{on}= 2.43±0.80 + 0.17±0.05V_{off} - 0.64±0.25W_y,
R^2= 5% df= 356 s= 5

◇ Model 3: U_{off}=-0.70±0.92 + 0.54±0.04U_{on}, R^2=25%
df= 552 s=22
V_{off}= 0.71±0.66 + 0.21±0.05V_{on}, R^2= 4%
df= 552 s=15

◇ Model 4: U_{on} =2.83±0.85 + 0.46±0.03U_{off}, R^2=25%
df= 552 s=20
V_{on}=2.14±0.57 + 0.16±0.04V_{off}, R^2= 4%
df= 552 s=13

◇ Model 5: U_{off}=1.77±1.31 + 2.92±0.27W_x, R^2=26%
df= 552 s=24
V_{off}=1.14±0.91 + 0.98±0.28W_y, R^2= 3%
df= 359 s=17

◇ Model 6: U_{on}= 5.37±1.40 + 1.27±0.28W_x, R^2= 6%
df= 331 s=25
V_{on}= 2.63±0.81 - 0.47±0.25W_y, R^2= 1%
df= 357 s=15

◇ Model 7: U_{off}-U_{on}=-3.61±1.44 + 1.66±0.29W_y,
R^2= 9% df= 331 s=26
U_{off}-U_{on}=-1.94±1.12 + 1.60±0.25W_y,(ECMWF)
R^2= 9% df= 422 s=23
V_{off}-V_{on}=-1.48±1.10 + 1.45±0.34W_x,
R^2= 5% df= 357 s=21

I have included values for the degrees of freedom, df, and the standard deviation of the residual, s. The former has been used to determine the 95% confidence limits of the regression coefficients. The percent of variance tabulated above and graphed in **Figure 13** is rather less than Poulain found. When stricter selection criteria were applied to the binned means used in this analysis, the percent of variance explained increased markedly, as will be seen later. Poulain selected data with buoy separations less than 10 km in space and less than 1 day in time, while buoy observations the 1-D analysis above were separated by less than 800 kilometers zonally, 200 kilometers meridionally and weeks in time. Results for individual models are separated in this figure by vertical dashed lines. Agreement was very good between results obtained by applying ECMWF or FNMOC winds to individual models, indicating that it makes very little difference which wind field is used. For the WOCE On/Navy Dataset, the constant term mostly evaluated to zero within 95% confidence limits, as shown in **Figure 14**. The regression coefficient, **C**, of buoy on (Navy buoy) drift on Navy buoy (buoy off) drift for this dataset was plotted against model and dataset in **Figure 15**. Generally, there is good agreement between values for a particular model applied to different datasets. The regression coefficient, **B**, of buoy drift on wind velocity shown in **Figure 16** is nearly zero for model 2, as one might expect since drogued buoy drift direction and velocity were tied to upper ocean currents, and could differ greatly from wind velocity and direction.

Next, the same models were tested with the binned WOCE On/Off Dataset; this dataset was drawn from 3001 pairs of 2° latitude by 8° longitude binned WOCE/TOGA drogue on and WOCE/TOGA drogue off velocity observations. The median number of observations in a bin was 75 and the maximum was 1679:

◇ Model 1: U_{off}=1.07±0.45 + 0.59±0.02U_{on} + 1.81±0.10W_x,
R^2=45% df=1709 s=17
V_{off}=0.27±0.29 + 0.31±0.03V_{on} + 1.07±0.10W_y,
R^2=11% df=1834 s=12

◇ Model 2: U_{on}=0.00±0.43 + 0.51±0.02U_{off} - 0.08±0.10W_x,
R^2=35% df=1709 s=16
V_{on}=0.11±0.24 + 0.22±0.02V_{off} - 0.41±0.09W_y,
R^2= 7% df=1834 s=10

◇ Model 3: U_{off}=-2.36±0.31 + 0.67±0.02U_{on},
R^2=33% df=2830 s=17
V_{off}=-0.29±0.22 + 0.26±0.02V_{on},
R^2= 5% df=2830 s=12

◇ Model 4: U_{on} =0.39±0.27 + 0.49±0.01U_{off},
R^2=33% df=2830 s=14
V_{on} =0.15±0.19 + 0.20±0.02V_{off},
R2= 5% df=2830 s=10

◇ Model 5: U_{off}=1.53±0.54 + 2.51±0.10W_x,
R^2=22% df=1727 s=20
U_{off}=1.91±0.43 + 2.72±0.10W_x (ECMWF),
R^2=27% df=2172 s=18
V_{off}=0.38±0.30 + 1.00±0.11W_y,
R^2= 5% df=1835 s=13
V_{off}=0.34±0.26 + 1.13±0.10W_y (ECMWF),
R^2= 6% df=2180 s=12

◇ Model 6: U_{on}=0.67±0.50 + 1.16±0.10W_x,
R^2= 7% df=1761 s=19
U_{on}=0.96±0.40 + 1.21±0.09W_x (ECMWF),
R^2= 8% df=2207 s=17
V_{on}=0.16±0.23 - 0.17±0.09W_y,
R^2=0.2% df=1886 s=11
V_{on}=0.13±0.23 - 0.17±0.08W_y (ECMWF),
R^2=0.2% df=2215 s=11

◇ Model 7: U_{off}-U_{on}=0.09±0.04 + 1.35±0.09W_x,
R^2=13% df=1710 s= 1.5
V_{off}-V_{on}=0.15±0.34 + 1.20±0.12 W_y,
R^2= 5% df=1835 s=14.

The percent of variance explained in this dataset by the first two models was very nearly the same as the models explained in the WOCE On/Navy Dataset (**Figure 13**). The constant term, **A**, evaluated to zero within 95% confidence limits for 13 out of 17 models applied to this dataset, as shown in **Figure 14**, and was very nearly zero within 95% confidence limits for two of the four remaining models. The first regression coefficient, **C**, sometimes was less than the corresponding coefficient found by Poulain (1994), as can be seen in **Figure 15**. Agreement between the WOCE On/Navy Dataset and the WOCE On/Off Dataset is very good for all models. The regression coefficient, **B**, of buoy drift on wind velocity are shown in **Figure 16** and agreed for any particular model regardless of dataset, except for model 1.

Finally, the regression cannot be expected to explain all of the variance in buoy drift due to wind. The limits on the ability to explain variance with the binned datasets has been explored by separating the WOCE On/Navy dataset into two independent subsets, computing the binned means and variances for both data subsets and then attempting to explain the variance of one binned subset in terms of the other. Results were that between 60% and 70% of the variance was explained by regressing a binned subset of WOCE drogued buoy drift velocity on another binned subset of the WOCE drogued buoy drift velocity. This implied that no 1-D analysis of the binned datasets could explain much more than 60% of the variance at best.

Wave drift has also been approximated from FNMOC wave height, direction, and period for every buoy location and time but the results are entirely negative; the inclusion of wave drift did not improve the predictability of any of the models. Such relationship as existed may be obscured by errors in the FNMOC wave field or that the wave field does not contain separate information from the winds on time scales less than several days.

In summary, results of these 1-D regression analyses are:

◇ For the purposes of this study, the constant term in the regression analysis, **A**, may be assumed to be zero;

◇ Both coefficients **B** & **C** and variance explained are the same within error for regressions using Navy buoy velocity or undrogued WOCE buoy velocity as dependent or predictor variables, i.e. the Navy buoys behave like undrogued WOCE buoys;

◇ The regression coefficients and variance explained are the same within errors for either FNMOC or ECMWF winds and for the purposes of this study, either FNMOC or ECMWF winds should be sufficient.

◇ Coefficients of dependence upon wind in WOCE buoys are nearly the same as found by Poulain (1994);

◇ The analysis should be geographically segregated and in particular low-shear areas should be selected for this analysis;

6.2 Two-dimensional Regression on Synoptic Data

Using the results of the 1-D study, a 2-dimensional regression model has been developed. We have let each buoy drift observation vector and each wind vector be a complex number; the real

part of the number is the north-south component of the vector and the imaginary part of the number is the east-west component of the vector. Following the results of the 1-D study in section 6.1, the coefficient **A** was set equal to zero. Having confirmed the dependence of undrogued drift upon drogued drift in the 1-D study, the regressions of undrogued(drogued) drift on drogued (undrogued) drift were eliminated. The 2-d regression analyses were done on two scales; first, the data in each 2° latitude by 8° longitude bin was used to calculate a regression of either six-hourly synoptic drogued or six-hourly synoptic undrogued buoy drift on synoptic undrogued wind:

$$u_{undrogued} = B_{undrogued} \cdot W_{undrogued}, \qquad (10)$$

$$u_{drogued} = B_{drogued} \cdot W_{undrogued}. \qquad (11)$$

Since we have been seeking the influence of the wind on the undrogued buoy, we therefore selected the wind at the position of the buoy most affected by the wind. However, the wind at the position of the undrogued buoy was constrainted to be within 1 m/s of the wind at the drogued buoy; results should be nearly independent of the choice of $W_{undrogued}$ or $W_{drogued}$ in the regression analysis. Each regression coefficient $\boldsymbol{B}$ is complex valued and the real and imaginary parts of $\boldsymbol{B}$ have meaning only in relation to the product of the buoy drift with the wind; the real part of $\boldsymbol{B}$ is the longitudinal component, parallel to the wind vector, and the imaginary part of $\boldsymbol{B}$ is the transverse component, orthogonal to the wind vector. If the wind was entirely east-west then any buoy drift predicted from the coefficient and the wind was east-west and north-south in proportion to the real and imaginary parts of the coefficient $\boldsymbol{B}$, respectively. The phase angle of the complex linear regression coefficient was therefore the angle of the response of the buoy drift to the wind.

In order to find the underlying relationship between the buoy drift and wind forcing, it was necessary to select from thousands of bins those which have the least error and bias. This was the advantage of dealing with a dataset of millions of observations; the underlying relationship between the buoy drift and wind existed at each observation point but was obscured by errors in the wind values, horizontal shear in upper ocean currents and other sources of random error. Only a subset of 27 selected bins was clear enough from these influences to enable the analysis to proceed. The selection criteria were that:

- ◇ The undrogued wind should explain over 60% of the variance of the undrogued buoy drift;
- ◇ The number of observations in a bin were at least 15 or more
- ◇ The percent of observations contributed by each buoy could not be more than 20% of the total. The latter criterion was suggested by previous experience with drifting buoy data analysis (P.P. Niiler, personal communication).
- ◇ In rare instances where the drogued buoy drift is highly correlated with the wind the deviant drift relationship is obscured - deviant drift becomes a small difference between two large numbers - and these instances were also rejected.
- ◇ Any instance of retrograde motion of an undrogued buoy was rejected on the grounds that such a dynamics was unphysical and probably represented an error in wind or buoy drift or both.

Each bin yielded an estimate of the complex coefficient B of the vector regression equation using singular-value decomposition and assuming a Gaussian normal error distribution.for binned mean drift deviations: Since each bin extended over only 2° of latitude, it was not necessary for this equation to have a term which depends upon the latitude. As will be explained later, the dependence on wind is best examined in terms of the phase and amplitude of the complex coefficients, rather than the real and imaginary parts. The results of this analysis are displayed in in terms of amplitude and phase of $B_{deviant}$ rather than real and imaginary components. Taking the difference of equation 10 and equation 11, we have:

$$\begin{aligned} u_{deviant} &= u_{undrogued} - u_{drogued} \\ &= B_{deviant} \cdot W_{undrogued} \qquad (12) \\ &= \left|B_{deviant}\right| \cdot e^{2\pi i\theta/360} \cdot W_{undrogued} \end{aligned}$$

The complex coefficient $B_{deviant}$ is the

difference between the coefficients $B_{undrogued}$ and $B_{drogued}$. θ is the phase of $B_{deviant}$ in degrees. **Figure 18 (bottom)** displays a scatterplot of amplitudes of $B_{deviant}$ vs. latitude for 27 selected bins; a least-squares best fit to a linear Ekman model of latitudinal variation of the amplitude of $B_{deviant}$ explains 34% of the variance in $B_{deviant}$. The model is explained in Section 6.3, below. Estimates of the 95% confidence limits of $B_{deviant}$ are shown in this figure; the mean confidence limit so estimated is approximately 0.1 cm/sec. We also computed the regression of binned mean $U_{deviant}$ on wind and a function of the Coriolis parameter, which solved the problem on a global scale, instead of the sub-bin scale for which equation 10 and equation 11 were solved as discussed above. Data was summarized by computing the mean and standard deviation of buoy drift, U_U and U_{15}, and wind, W, in the every bin; the first 1-dimensional regression results were derived from such summaries. The 2-dimensional analyses used similar summaries, which differ in that they included cross-variance statistics like:

$$\overline{u_u \cdot W^*}; \quad \overline{u_{15} \cdot W^*},$$

where u_u, u_{15}, and W were six-hourly synoptic buoy drift and wind, the * denotes complex conjugation, and means were over all time. These results explained over 47% of the variance in the amplitude of $u_{deviant}$ if a term explaining latitudinal variability was included. In order to explain these results more completely it is now necessary to examine the nature of this latitudinal variability in more detail

6.3. Ekman Currents and Latitude Dependence

In order to develop a model of the latitudinal dependence of the relationship between deviant drift and wind stress, the theoretical relationship between near surface currents and wind must be examined. The momentum balance of large spatial scale, time-mean near surface circulation of the ocean is a linear relationship between the Coriolis force, pressure gradient and the vertical convergence of the turbulent stress due to the winds (Pedlosky, 1979).

$$\rho \cdot f \cdot \vec{u} = -g\rho_0 \vec{\nabla}\eta + \frac{\partial \vec{\tau}}{\partial z}. \qquad (13)$$

When the local pressure gradient is not statistically or dynamically related to the local wind (Niiler et al., 1993; Luther et al., 1990) and it can be estimated from sea level or hydrographic measurements (Ralph and Niiler, 1997), it is, in principle, possible to estimate the vertical convergence of the wind-produced turbulent stress from the ageostrophic component of the current. This convergence of stress depends upon the processes by which vertical, turbulence transports of momentum occur on time scales shorter than the time scale at which the Ekman balance ensues. Ralph and Niiler (1997) have made an analysis of the ensemble mean ageostrophic circulation measured by WOCE drifters at 15m depth in the tropical Pacific. They found that the best statistical model (49% of variance explained) was one in which the both the amplitude of the current and its vertical scale were proportional to wind speed and inversely proportional to the square root of the Coriolis parameter, $f=1.458\times10^{-4}(sec.^{-1})$ sin(latitude). When the ageostrophic currents at 15m depth were plotted as functions of a non-dimensional depth equal to 15m, divided by the scale depth, an increasing rotation to the right of the wind was observed as a function of this scaled, non-dimensional depth. The scale depth (L) is in general a very complex functional of the generation, transport, and dissipation of mechanical and potential energy. However, an examination of scale depth in various limits provides a conceptual guide for the development of our statistical model. In the presence of strong winds non-stratified turbulence scales apply (e.g. Caldwell et al., 1972): $q \sim u^*$; $L \sim u^*/f$; $A \sim u^{*2}/f$. In the presence of strong buoyancy fluxes, B, Monin-Oubokov scalings are appropriate (McPhee, 1995) $L \sim u^{*3}/-B$. From these limiting scaling arguments it can be shown that for non-stratified, turbulent layers the Ekman currents are proportional to wind speed and the scale depth is proportional to wind speed divided by the Coriolis paramenter: $u_E \sim u^*$; $H_E \sim u^*/f$. This is the limiting case during the winter season in sub-polar gyres. During times of strong heating and light winds, as occur in spring and early summer for the establishment of the seasonal thermocline, the length scale is proportional to Monin-Oubokov scale. These results imply the remarkable result that the Ekman currents are independent of wind and their depth scale is proportional to the wind speed squared: $u_E \sim (-B/f)$, $H_E \sim u^{*2}/(-Bf)$; under these special conditions the model for deviant drift may not work. The physics that lead to the most statistically useful scaling in the tropical Pacific is

a third limit. In this limit mixing of a negative buoyancy flux is done by shear of the near-inertial currents, as would occur in late Summer conditions in the mid-latitude oceans, where a weak stratification, N, is maintained:

$$u_E \sim u^*/(f/N)^{1/2}\ ;$$

$$H_E \sim u^*/(Nf)^{1/2}\ ; \qquad (14)$$

In summary, in the most generally applicable model of Ekman currents, they are proportional to wind speed and inversely proportional to the square root of the Coriolis parameter. This analysis is appropriate for the computation of long term mean Ekman currents, although in cases of strong negative buoyancy fluxes, the linear dependence of current on wind speed will weaken and be difficult to establish statistically (personal communication, P.P. Niiler).

Following the above analysis the equation for the latitudinal dependence of the coefficient B in equation 12 can be rewritten:

$$u_{deviant} = (B_0 + B_1 \cdot f^{-1/2}) \cdot e^{2\pi i\theta/360} \cdot W_{undrogued}, \qquad (15)$$

$$\theta = \theta_0 + \theta_1 \cdot |W_{undrogued}| \cdot f^{-1/2}$$

where $u_{deviant}$ and $W_{undrogued}$ are complex valued, but all other parameters are real valued. Observed amplitudes of $|B|$, are plotted versus latitude in **Figure 18 (bottom)** and can be used to solve for the amplitude of the coefficients in equation 15, assuming the complex phase θ of B_0 and B_1 are identical. This is essential since the theoretical analysis above has shown that θ varies inversely with the scale depth, and the scale depth is a linear function of both the wind speed, W, and the reciprocal of the square root of the Coriolis parameter, $f^{-1/2}$. A regression analysis of the expression in parenthesis in equation 15 gives B_0=-0.257 (cm/m), B_1=0.01576 (cm/m sec$^{1/2}$), where f, is the Coriolis parameter. There was evidence that the standard error of the coefficients returned by this regression overestimates the error over much of the latitude range because the envelope of points in Figure 18 (bottom) expands from lower to higher latitudes. Taking this into account and disregarding five extreme outliers, the values of B converge to an amplitude of 2 at 20° latitude and are enveloped by an lower curve (upper curve for absolute latitudes less than 20°) described by B_0=-1.72 (cm/m), B_1=0.02556 (cm/m sec$^{1/2}$) and an upper curve (lower curve for absolute latitudes less than 20°) described by B_0=0.894 (cm/m), B_1=0.00852 (cm/m sec$^{1/2}$). The envelope enclosed over 80% of the data and was used to make an estimate of confidence limits for the amplitude of the wind coefficient. The difference in the lower and upper bounds of the wind coefficient |B| defined the longitudinal axis of an error ellipse:

$$\varepsilon_{B\|} = \left|2.614 - 0.01704 \cdot f^{-1/2}\right|; \quad if\ \varepsilon_{B\|} \geq .1$$
$$\varepsilon_{B\|} = .1; \quad otherwise \qquad (16)$$

$\varepsilon_{B\|}$ wasn't allowed to be smaller than 0.1, derived from the average 95% confidence of |B| values shown in Figure 18 (bottom). It follows that the longitudinal axis of the deviant drift error ellipse (along the direction of U_D) was:

$$\varepsilon_{U_D\|} = \varepsilon_{B\|} \cdot |W|. \qquad (17)$$

The error will be discussed further in Section 6.5, below.

6.4 Two-dimensional Regression on Binned Means

As has been mentioned, a regression was also made of binned mean drift deviation on binned mean undrogued buoy wind; this analysis assumes the relationship shown in equation 14 held for mean buoy drift and mean wind, just as it did for synoptic buoy drift and synoptic wind. A scatterplot of the mean deviant buoy drift vs. the mean undrogued buoy wind for the same selected bins as used in the analysis above is shown in **Figure 18(top)**; because no latitudinal dependence is included, the plot shows a trend equivalent to a low absolute B-value of 0.87. Including latitudinal dependence would require a 3-dimensional graph; the complex multiple regression equation is:

$$\overline{u_{deviant}} = (b_0 + b_1 \cdot f^{-1/2}) \cdot \overline{W_{undrogued}} \qquad (18)$$

The complex b_0 and b_1 coefficients in this

equation cannot reproduce the variation in θ which can be explained by equation 15 and therefore solutions to equation 18 fail to that extent. The full solution of equation 18 for binned means is displayed in **Figure 18(bottom)** as the dashed line indicating the regression on binned means (A=0). As can be seen, the solution is very close to the best fit to the regression coefficients computed from six-hourly synoptic data. As a check on the assumption of no constant term in equation 12, I have also plotted the regression on binned means assuming A≠0. These regressions explain over 47% of the variance.

6.5 Angle of Response

The angle of response, θ, of undrogued WOCE and Navy buoy drift deviation to vector wind is shown in **Figure 19**. The angle of response is the phase angle of the complex ***B*** coefficient, given by

$$\theta = ArcTan(\mathrm{Im}aginary(B)/\mathrm{Re}al(B)) \quad (19)$$

For heuristic reasons, I have displayed the scatterplot of the response angle derived from synoptic data vs. latitude in **Figure 19 (top)**; no relationship can be seen between the angle and latitude. However, as shown in the discussion in section 6.3, equation 14, the angle depends upon both the Ekman depth and the inverse square-root of the Coriolis parameter. The relationship in equation 14 suggested **Figure 19 (bottom),** which shows a clear dependence of the response angle upon the product of the wind and the reciprocal of the square root of the sine of the latitude. This quantity, ξ, is proportional to the Ekman depth, H_E, defined in equation 14. Scatter is still great and the percent of variance explained in this figure is low, but a Student's T-test shows that the trend exists with greater than 95% confidence. Deviation from the trend in this figure may be because the relationship does not hold under all ocean conditions. No clear estimate of the variation of the angle of response with latitude could be obtained from the binned mean regression analyses; this is not surprising since it is obvious this complex regression would only show a clear relationship if there were a clear trend in **Figure 19 (top)**. The best estimate of a fixed angle of response from this analysis is approximately 25°, in the middle of the range of observed angles.

The range of the angles of response shown in **Figure 19** at any latitude was 10°; the precision of this estimate could be improved but not the accuracy. The transverse axis of the error ellipse for B is:

$$\varepsilon_{B\neg} = 0.1745 \cdot |B|, \quad (20)$$

Therefore the transverse axis of the deviant drift error ellipse was:

$$\varepsilon_{U_D\neg} = \varepsilon_{B\neg} \cdot |W|. \quad (21)$$

Equation 17 and equation 21 were used to estimate error in the Auxiliary Lagrangian Drift Dataset (ALDD), see Section 7.1, below.

6.6 Confirmation of Exponential Dependence

As has been discussed earlier (see section 6.3) we expect the deviant buoy drift to be proportional to the reciprocal of the square-root of the Coriolis parameter. We have tested the assumption that the exponent should be -1/2 and show the results in **Figure 20**. The amplitude of the regression coefficients, |B|, obtained from the synoptic analyses are modeled by the equation

$$|B| = B_o + B_1 \cdot \sin(latitude)^e \quad (22)$$

where values of |B| were taken from the observed coefficients for selected bins (section 6.2). Rearranging terms and taking the natural logarithm of both sides of the equation reveals a regression equation which can be solved for B and e:

$$\ln(B - B_o) = \ln B_1 + e\ln(\sin(latitude)) \quad (23)$$

B_o is set to -1, which is greater than its lower bound (see Section 6.3, above) and the equation is solved for e, a process equivalent to finding the best straight-line fit to the scatterplot in **Figure 20**. The results indicated e=-.53 was an optimal fit.

6.7 Complex (2-D) Buoy-pair Analysis

In the previous 2-D analyses there was a possible bias because drogued and undrogued observations are not drawn from identical populations. There is no restriction other than the data for undrogued (Navy) buoys and drogued buoys be drawn from the same bin; the data could be drawn from different years or from different

parts of a 2° latitude by 8° longitude bin. In order to test the possible effect of such bias we selected a sub-population of undrogued(Navy)-drogued drifter pairs separated by less than 50 km threshold distance and a time separation of 2 days. An important issue has been how close together an undrogued and drogued buoy must be before the undrogued buoy can be used to predict the drift of the drogued buoy. Global 2-dimensional linear regressions of undrogued (or Navy) buoy drift upon drogued buoy drift were done for several separation thresholds. Both the real and imaginary linear coefficients appear to reach an asymptotic value as the threshold separation becomes less than 50 km. This spatial separation was also selected based upon structure function results (see above); the time separation was selected because it was the spatial scale of synoptic disturbances in the atmosphere and previous experience with drifting buoys (P.P. Niiler, personal communication). Just as with the analyses in sections 6.2 through section 6.4, the regression was made both with synoptic data and with binned mean data. The distribution of observations is shown in **Figure 21 (top)**; selecting drifter pairs reduces the number of observations available to the analysis, a histogram of the number of observations in selected bins , displayed in **Figure 21 (bottom)**, shows that there were generally less than 100 observations of buoy pairs in a single 2° latitude by 8° longitude bin. Bins were selected only if they contained more than 5 observations and the wind explained more than 20% of the undrogued buoy drift velocity. Because of the buoy-pairing it was not possible to limit the number of observations contributed by a single buoy to 20% or less of the total in a single bin, as was done before. The distribution of selected buoy-pair bins is concentrated in lower latitudes compared to the distribution of binned means in **Figure 17 (top).** A scatterplot of buoy-pair deviant drift vs. wind is shown in **Figure 22**; the results of the complex 2-D regression on these selected binned means explained 34% of the variance. The absolute value of B, 1.58, is approximately what was found in earlier analyses, but the latitudinal variability is nearly nil; the angle of response is similarly indeterminate with large error. We have concluded that the number of observations, the bin spatial distribution, and the frequent reliance of bin means on data from a single buoy combine to make the buoy-pair analysis difficult. The absolute value of B obtained from the buoy-pair analysis is approximately what would be expected from the results shown in **Figure 18** and serves to that extent to confirm that bias has not aliased results discussed in earlier sections.

7. Products and Deliverables

7.1 The Auxiliary Lagrangian Drifter Datasett (ALDD)

We now have the capability of increasing the drift buoy dataset 50% by including observations of buoys which have lost their drogues; the same analysis which has made this possible will also support accurate estimates of the error in the drift buoy dataset. The comparison study has made Lagrangian velocity estimates from 177,938 observations of Naval AN/WSQ-6 drift buoys and 432,475 observations of undrogued WOCE/TOGA drifting buoys. Subtracting the predicted deviant drift, u_D, from undrogued buoy drift, u_u produced an estimate of Lagrangian current at 15 m, the drogue depth of the drogued buoys. The creation of the Auxiliary Lagrangian Drifter Dataset has increased the number of WOCE buoy drift vectors by less than the total of 848,416 undrogued buoy observations because estimates were made only when both ECMWF and FNMOC winds were available. Estimates made from Navy buoy drift have added 177,938 more observations out of a potential 192,140, many in regions not sampled by the WOCE buoy dataset. Just as importantly, error estimates were made from Equation 17 and Equation 20. The ALDD is available from Ocean Prospects on 4 mm DAT for cost. Copies of the ALDD have also been provided to FNMOC in Monterey, California and NRL at the Stennis Space Center, Mississippi.

7.2 The Picture Archive

After re-organizing the drifter buoy datasets into 2°x8° bins, I created a picture archive of drogued buoy - undrogued (or Navy) buoy pairs; while not specified in the contract, it is available as an overview tool. The area around each undrogued buoy observation or Navy buoy observation has been searched out to 300 km and the nearest drogued buoy observation at that synoptic time has been paired with the undrogued/Navy buoy observation. The archive is a Claris filemaker archive.

8. References

Caldwell, D., C.W. Van Atta, and K. Holland, A laboratory study of the turbulent Ekman boundary layer, *Geophys. Fluid Dyn.*, **3**, 123-160, 1972.

Ekman, V.W., On the influence of the Earth's rotation on ocean-currents, *Ark. Mat. Ast. Fys.*, **2**, 1-52, 1905.

Luther, D., A. Chave, J. Filloux, and P. Spain, Evidence for local and non-local barotropic responses to atmospheric forcing during BEMPEX, *Geophys. Res. Letts.*, **17**, 949-952, 1990.

Niiler, P.P., R.E. Davis, and H.J.White, 1987. Water-following characteristics of a mixed-layer drifter. *Deep-Sea Research*, **34**, 1867-1881.

Niiler, P.P., J.D. Paduan, A.L. Sybrandy and L. Sombardier, 1991. *The WOCE/TOGA Lagrangian surface drifter*. Proceedings of Oceans 91, Hawaii, October 91, 839-843.

Niiler, P., J. Filloux, W. Liu, R.M. Samuelson, Wind forced variability of the deep eastern North Pacific: Observations of sea floor pressure and abyssal currents. *J. Geophys. Res.*, **98**, 22589-22602, 1993.

Niiler, P.P., A.L. Sybrandy, K. Bi, P. Poulain, and D. Bitterman, 1995. Measurements of the water-following capability of holey-sock and TRISTAR drifters.. *Deep-Sea Research*, **42**, No. 11/12: 1951-1964.

Poulain, P.-M. and D.V. Hansen, 1996. Quality control and interpolation of WOCE/TOGA drifter data. *J. Atm.Oc.Tech.* **13**, 900-909.

Ralph, E.A., and P.P. Niiler, Wind driven currents in the tropical Pacific, *J. Phys. Ocean.*, in press, 1998.

Selsor, H.D., 1993. Data from the sea: Navy drift buoy program. *Sea Technology*. December, 1993, 53-58.

Pedlosky, J., *Geophysical Fluid Dynamics*. New York:Springer-Verlag, 1982. 623 pp.

Poulain,P.-M.. Talk delivered at the 7th WOCE/TOGA Surface Velocity Program Meeting (SVP7) at La Jolla, November 2-4, 1994.

Poulain,P.-M., A. Warn-Varnas, and P.P. Niiler, 1996. Near-surface circulation of the Nordic seas as measured by Lagrangian drifters. *JGR*, **101**, No. C8: 18,237-18,259.

Sombardier, L. and P. Niiler. Talk delivered at the 7th WOCE/TOGA Surface Velocity Program Meeting (SVP7) at La Jolla, November 2-4, 1994.

APPENDIX A- DRIFT BUOY DESIGN

A1. Naval AN/WSQ-6 Drifters

METOCEAN Data Systems, Ltd., of Halifax, Nova Scotia, Canada manufactures the Naval AN/WSQ-6 drifter shown in **Figure A.1**. The Naval Research Laboratory's (NRL) Tactical Oceanographic Warfare Support (TOWS) Program has managed and evaluated development of the Naval AN/WSQ-6 buoys (Selsor, 1993). They are self-contained drifters designed for a minimum of 90 days unattended collection of oceanographic and meteorological data from the open ocean; the deployed physical dimensions of the Naval AN/WSQ-6 [6] drifter appear in **Table A.1**. The Naval AN/WSQ-6 buoy comes in a sonobuoy style package; it samples air temperature, sea surface temperature and barometric pressure hourly and transmits these data in Service ARGOS formats through NOAA polar orbiting satellites. Since platform position is determined by the Doppler shift in the ARGOS satellite carrier wave frequency, buoy positions can be estimated only during a satellite overpass, generally no more than twice a day. In January 1991, the U.S. Navy endorsed an operational requirement for development of a new Naval AN/WSQ-6 type buoy, to come in three variations. Since then the new buoy has been under development and as of May 1994 the last of the Naval AN/WSQ-6 I buoys had been deployed. The intercomparison would include data from the two principal manufacturer's versions of the Naval AN/WSQ-6, the CMOD and CMOD-I, although heavily weighted towards the former.

An important factor in Lagrangian drifter design is the "*drag area ratio*," which is the ratio of the drag area of the drogue to the sum of the drag areas of the tether system, submerged floats, and hull (see section 3.2). Drag area is the frontal area of a buoy component times its drag coefficient. A drag area ratio larger than 30 is needed for small "slip", the difference of velocity of the drifter and vertically integrated current velocity; drag areas of each component of the Naval AN/WSQ-6 drifter and the drag area ratio of the drifter are tabulated in **Table A.1.** Although the Naval AN/WSQ-6 drag area ratio is insufficient for a Lagrangian drifter, a Naval AN/WSQ-6 buoy designed to be influenced by surface wind and wave is desirable for meteorological purposes (Kreitzberg, *personal communication*).

Naval AN/WSQ-6 drifters are air deployed from P-3 aircraft, S-3 patrol aircraft, and various helicopter platforms (Selsor, 1993). The Naval AN/WSQ-6 buoy is drogued, usually with the aluminum cylindrical container used for packaging prior to deployment, capped at both ends and weighing 12.4 kg; a short wire cable connects it to the nylon tether which is attached in turn to a toroidal surface flotation collar surrounding the buoy proper. Over 95% of the total number constructed conform to this plan, although several variants have been proposed and built (ibid., 1993; METOCEAN, *personal communication*); moreover, buoys deployed by the Navy conform to this plan even more consistently. Most recently, however, the flotation device has been enlarged; CMOD-II, built after May 1, 1994, must be considered as having quite different surface drag characteristics. The original Naval AN/WSQ-6 buoy was tethered with a 100' nylon line; the CMOD-II version is tethered with a 4 meter nylon line protected with VEXAR H-30 fish netting. Approximately 1500 of the Naval AN/WSQ-6 buoys have been made since 1989, with over 1200 going to the U.S. Navy, the rest to research programs and foreign navies.

All Naval AN/WSQ-6 buoys are adaptable to several configurations (Selsor, 1994). The float assembly in each of these is the same, but the drogue, antenna and sensor arrangements differ; the configurations are further complicated by the presence or absence of protective netting on the tether and surface float variants. As mentioned before, the CMOD II surface float was larger than the CMOD I surface float. Further modifications may be planned, including a version that includes an Aanderaa Instruments acoustic Doppler sensor that will directly measure slip velocity . These float-drogue configurations would have its unique drag area ratio and its own response to wind and wave forcing; drag area ratio will parametrize the wind and wave response, extending the results of this study to a variety of drifters. Drag area ratio remains the most likely candidate for the appropriate dimensionless shape factor if only because of past success in applying it to these problems; however, there are other possible dimensionless factors, such as those associated with tether vibration or drogue lift.

[6] This is the latest version of the Naval AN/WSQ-6 drifter, designated the CMOD-II by METOCEAN and built after May 1, 1994.

A2. WOCE/TOGA Drifters

The World Ocean Circulation Experiment (WOCE) and the Tropical Ocean and Global Atmosphere (TOGA) Program have established a long term ocean observing system for monitoring ocean currents; this program, called the Surface Velocity Program (SVP), coordinates global deployment of Lagrangian drifters. In the United States, this is done principally from the Global Drifter Center (GDC) at the Scripps Institution of Oceanography. The SVP has been deploying over 300 drifters per year since about 1991, principally in the global tropics (Niiler *et alia*, 1991). Considerable effort has gone into designing a Lagrangian drift buoy used in the SVP (Niiler *et alia,* 1987). The WOCE/TOGA SVP Lagrangian drifter, shown in **Figure A.2,** is light-weight, constructed of low-cost sea water compatible plastics; it is composed of a surface float, a tether and a drogue. Plastic impregnated wire rope tethers the surface float to the drogue. Its physical characteristics, including its drag area ratio, are tabulated in **Table A.2** (Niiler et al., 1991). It has a mean time before failure of about one year, and it is easy to deploy from Volunteer Observing Ships (VOS). It is designed to follow water parcels vertically averaged over a drogue of height 6-7 m, centered 15 m below the surface (WCRP-26); the drag area ratio is an order of magnitude greater than the Naval AN/WSQ-6 buoys, as can be seen by comparing **Table A.1** and **Table A.2**. There were two principal design considerations: 1. the drogue slip should be predictable; 2. the drifter should have a mean time to failure of many months in an open ocean environment. As a consequence, the final design incorporates the following features: 1. three dimensionally symmetric float and drogue; 2. thin and stiff wire tether; 3. dimensionally stable drogue with a high drag coefficient, the holey sock drogue, and 4. drag area ratio of 38. These features act to reduce the steady tension and eliminate any shock stress between surface and subsurface elements of the drifter, minimize surface wave effects, and reduce the drag of the tether and submerged floats relative to the drag of the drogue. During tests, a Velocity Measuring Current Meter (VMCM) attached to the top and bottom of the drogue did not measure slip greater than 1 cm/sec in conditions of 10 m/sec winds.

There are several manufacturers of these buoys and many variants on the buoy described in Table A.2 in the Ocean Prospects data archive. The variant buoys are named Holeysock', 'Ministar', 'Tristar', 'Window Shade', and 'Sheet' after the style of their drogues. However, drogue type does not vary as much as other parts of the buoys; the most variable component is the tether strain relief linkage. A summary by tether strain relief linkage finds that the the great majority of buoys are Holeysock buoys with Urethane carrots at all float-tether connections. Clearwater and Technocean buoys make, being well-tested and well-understood, and adhering to this standard design, were selected from the buoy dataset; all other buoys will be excluded from the analysis for the purpose of maintaining consistency.

APPENDIX B. GF-3 SOFTWARE

The GF-3 system was developed by the IOC Working Committee on International Oceanographic Data Exchange (IODE) as a generalized formatting system for the exchange and archival of data within the international oceanographic community. Two computer experts, Roy K. Lowry and Trevor Sankey of the British Oceanographic Data Centre, have developed software for reading and writing data in the GF-3 format (IOC, 1989). I obtained versions of this software from Roy Lowry which had been written for use with the DOS and UNIX operating systems and adapted it to ABSOFT Fortran on a Power Macintosh 7100/66 running Mac OS 7.5. The MEDS Naval buoy dataset was stored in an idiosyncratic variation of the GF-3 format, which required some adaptation to the GF-3 level 4 software in order to read it. This adaptation is obtainable by request from Ocean Prospects and will be part of the software delivered to the Navy at the end of the present project.

Roy Lowry is at Bidston Observatory, Birkenhead, MERSEYSIDE L43 7RA, UK; however, it is best to contact him via E-mail at:

rkl@unixa.nerc-bidston.ac.uk

APPENDIX C. GRIB SOFTWARE

John D. Stackpole, Automation Division, National Meteorological Center has written a reference to GRIB, the WMO format for the storage of weather product information and the exchange of product messages in gridded binary form. The edition 1 guide to GRIB is contained in a file called format_grib on. In Stackpole's words, "the World Meteorological Organization (WMO) Commission for Basic Systems (CBS) Extraordinary Meeting Number VIII (1985) approved a general purpose, bit-oriented data exchange format, designated FM 92-VIII Ext. GRIB (Gridded Binary). It is an efficient vehicle for transmitting large volumes of gridded data to automated centers over high speed telecommunication lines using modern protocols. By packing information into the GRIB code, messages can be made more compact than character oriented bulletins, which will produce faster computer-to-computer transmissions. GRIB can equally well serve as a data storage format, generating the same efficiencies relative to information storage and retrieval devices." GRIB software can be downloaded via anonymous FTP from nic.fb4.noaa.gov; the GRIB document guide.txt is in the directory pub/nws/nmc/docs/gribguide; other documentation and code is in the directory ./pub/nws/nmc/codes/grib.wafs/. My software for reading the FNMOC archived fields is available by request to Ocean Prospects and will be part of the software delivered to the Navy at the end of the present project.

APPENDIX D. INTERPOLATION IN TIME

A worm track of a selected Naval AN/WSQ-6 drift buoy, ARGOS 12501, deployed in May, 1990, is shown in **Figure D.1**. Numbered and shaded circles indicate where linear interpolation was not effective. **Figure D.2** displays interpolated and observed Navy buoy latitude (top) and longitude (bottom) versus time. Cusps (turning points) can be observed in latitude vs. time (top) at (1), (2), and (5), and a discontinuous "jog" is apparent at (3); cusps are at (3) and (4) in longitude vs. time (bottom). Meridional and zonal velocity can be computed by finite differences from the interpolated and observed positions and times. In **Figure D.3**, meridional (top) and zonal (bottom) buoy velocity components from interpolated and observed positions compare well except at the numbered positions. As a consequence of these problems, and in order to maintain consistency between analyses, I will use software developed at the Scripps Institution of Oceanography, by Dr. Pim Van Meurs, the Principal Components Interpolation Method (PIM) software which uses an decomposition into inertial and tidal modes to make objective interpolations and extrapolations of position observations. This software, as adapted for use with the Navy drift buoy dataset will be available from Ocean Prospects.

APPENDIX E. ASYMPTOTIC VALUE OF VARIANCE

TABLE I. Estimated asymptotic value of variance of buoy pair ECMWF wind differences in rectangular regions of the globe as the buoy pair separation decreases to zero.

PARAMETER NAME	DATASET	CORNERS OF RECTANGULAR REGION (LATITUDE,LONGITUDE)	(LATITUDE,LONGITUDE)	VARIANCE			UNITS
ZONAL ECMWF	NAVY/WOCE	(30°S, 0°E)	(0°N, 100°E)	10	±	5	(m/s)**2
ZONAL ECMWF	NAVY/WOCE	(30°S, 100°E)	(0°N, 180°E)	20	±	10	(m/s)**2
ZONAL ECMWF	NAVY/WOCE	(30°S, 180°E)	(0°N, 280°E)	30	±	15	(m/s)**2
ZONAL ECMWF	NAVY/WOCE	(30°S, 280°E)	(0°N, 360°E)	10	±	5	(m/s)**2
MERIDIONAL ECMWF	NAVY/WOCE	(30°S, 0°E)	(0°N, 100°E)	10	±	5	(m/s)**2
MERIDIONAL ECMWF	NAVY/WOCE	(30°S, 100°E)	(0°N, 180°E)	20	±	10	(m/s)**2
MERIDIONAL ECMWF	NAVY/WOCE	(30°S, 180°E)	(0°N, 280°E)	20	±	15	(m/s)**2
MERIDIONAL ECMWF	NAVY/WOCE	(30°S, 280°E)	(0°N, 360°E)	10	±	5	(m/s)**2
ZONAL ECMWF	NAVY/WOCE	(0°N, 0°E)	(30°N, 100°E)	60	±	20	(m/s)**2
ZONAL ECMWF	NAVY/WOCE	(0°N, 100°E)	(30°N, 180°E)	120	±	40	(m/s)**2
ZONAL ECMWF	NAVY/WOCE	(0°N, 180°E)	(30°N, 280°E)	120	±	40	(m/s)**2
ZONAL ECMWF	NAVY/WOCE	(0°N, 280°E)	(30°N, 360°E)	100	±	40	(m/s)**2
MERIDIONAL ECMWF	NAVY/WOCE	(0°N, 360°E)	(30°N, 100°E)	60	±	20	(m/s)**2
MERIDIONAL ECMWF	NAVY/WOCE	(0°N, 100°E)	(30°N, 180°E)	120	±	40	(m/s)**2
MERIDIONAL ECMWF	NAVY/WOCE	(0°N, 180°E)	(30°N, 280°E)	120	±	40	(m/s)**2
MERIDIONAL ECMWF	NAVY/WOCE	(0°N, 280°E)	(30°N, 360°E)	100	±	40	(m/s)**2
ZONAL ECMWF	NAVY/WOCE	(30°N, 0°E)	(60°N, 100°E)	60	±	40	(m/s)**2
ZONAL ECMWF	NAVY/WOCE	(30°N, 100°E)	(60°N, 180°E)	200	±	50	(m/s)**2
ZONAL ECMWF	NAVY/WOCE	(30°N, 180°E)	(60°N, 280°E)	200	±	50	(m/s)**2
ZONAL ECMWF	NAVY/WOCE	(30°N, 280°E)	(60°N, 360°E)	180	±	50	(m/s)**2
MERIDIONAL ECMWF	NAVY/WOCE	(30°N, 360°E)	(60°N, 100°E)	60	±	40	(m/s)**2
MERIDIONAL ECMWF	NAVY/WOCE	(30°N, 100°E)	(60°N, 180°E)	200	±	50	(m/s)**2
MERIDIONAL ECMWF	NAVY/WOCE	(30°N, 180°E)	(60°N, 280°E)	200	±	50	(m/s)**2
MERIDIONAL ECMWF	NAVY/WOCE	(30°N, 280°E)	(60°N, 360°E)	180	±	50	(m/s)**2

TABLE II. Estimated asymptotic value of variance of buoy pair FNMOC wind differences in rectangular regions of the globe as the buoy pair separation decreases to zero.

PARAMETER NAME	DATASET	CORNERS OF RECTANGULAR REGION (LATITUDE,LONGITUDE)	(LATITUDE,LONGITUDE)	VARIANCE	±		UNITS
ZONAL FNMOC	NAVY/WOCE	(30°S, 0°E)	(0°N, 100°E)	10	±	5	(m/s)**2
ZONAL FNMOC	NAVY/WOCE	(30°S, 100°E)	(0°N, 180°E)	20	±	10	(m/s)**2
ZONAL FNMOC	NAVY/WOCE	(30°S, 180°E)	(0°N, 280°E)	30	±	15	(m/s)**2
ZONAL FNMOC	NAVY/WOCE	(30°S, 280°E)	(0°N, 360°E)	10	±	5	(m/s)**2
MERIDIONAL FNMOC	NAVY/WOCE	(30°S, 0°E)	(0°N, 100°E)	10	±	5	(m/s)**2
MERIDIONAL FNMOC	NAVY/WOCE	(30°S, 100°E)	(0°N, 180°E)	20	±	10	(m/s)**2
MERIDIONAL FNMOC	NAVY/WOCE	(30°S, 180°E)	(0°N, 280°E)	20	±	15	(m/s)**2
MERIDIONAL FNMOC	NAVY/WOCE	(30°S, 280°E)	(0°N, 360°E)	10	±	5	(m/s)**2
ZONAL FNMOC	NAVY/WOCE	(0°N, 0°E)	(30°N, 100°E)	60	±	20	(m/s)**2
ZONAL FNMOC	NAVY/WOCE	(0°N, 100°E)	(30°N, 180°E)	120	±	40	(m/s)**2
ZONAL FNMOC	NAVY/WOCE	(0°N, 180°E)	(30°N, 280°E)	120	±	40	(m/s)**2
ZONAL FNMOC	NAVY/WOCE	(0°N, 280°E)	(30°N, 360°E)	100	±	40	(m/s)**2
MERIDIONAL FNMOC	NAVY/WOCE	(0°N, 360°E)	(30°N, 100°E)	60	±	20	(m/s)**2
MERIDIONAL FNMOC	NAVY/WOCE	(0°N, 100°E)	(30°N, 180°E)	120	±	40	(m/s)**2
MERIDIONAL FNMOC	NAVY/WOCE	(0°N, 180°E)	(30°N, 280°E)	120	±	40	(m/s)**2
MERIDIONAL FNMOC	NAVY/WOCE	(0°N, 280°E)	(30°N, 360°E)	100	±	40	(m/s)**2
ZONAL FNMOC	NAVY/WOCE	(30°N, 0°E)	(60°N, 100°E)	60	±	40	(m/s)**2
ZONAL FNMOC	NAVY/WOCE	(30°N, 100°E)	(60°N, 180°E)	200	±	50	(m/s)**2
ZONAL FNMOC	NAVY/WOCE	(30°N, 180°E)	(60°N, 280°E)	200	±	50	(m/s)**2
ZONAL FNMOC	NAVY/WOCE	(30°N, 280°E)	(60°N, 360°E)	180	±	50	(m/s)**2
MERIDIONAL FNMOC	NAVY/WOCE	(30°N, 360°E)	(60°N, 100°E)	60	±	40	(m/s)**2
MERIDIONAL FNMOC	NAVY/WOCE	(30°N, 100°E)	(60°N, 180°E)	200	±	50	(m/s)**2
MERIDIONAL FNMOC	NAVY/WOCE	(30°N, 180°E)	(60°N, 280°E)	200	±	50	(m/s)**2
MERIDIONAL FNMOC	NAVY/WOCE	(30°N, 280°E)	(60°N, 360°E)	180	±	50	(m/s)**2

TABLE III. Estimated asymptotic value of variance of Navy buoy pair drift velocity differences in rectangular regions of the globe as the buoy pair separation decreases to zero. There is some tendency for the asymptotic buoy drift variance to increase northwards;

PARAMETER NAME	DATASET	CORNERS OF RECTANGULAR REGION (LATITUDE,LONGITUDE)	(LATITUDE,LONGITUDE)	VARIANCE	±		UNITS
ZONAL DRIFT	NAVY	(30°S, 0°E)	(0°N, 100°E)	250	±	75	(cm/s)**2
ZONAL DRIFT	NAVY	(30°S, 100°E)	(0°N, 180°E)	250	±	100	(cm/s)**2
ZONAL DRIFT	NAVY	(30°S, 180°E)	(0°N, 280°E)	250	±	100	(cm/s)**2
ZONAL DRIFT	NAVY	(30°S, 280°E)	(0°N, 360°E)	200	±	100	(cm/s)**2
MERIDIONAL DRIFT	NAVY	(30°S, 0°E)	(0°N, 100°E)	250	±	150	(cm/s)**2
MERIDIONAL DRIFT	NAVY	(30°S, 100°E)	(0°N, 180°E)	250	±	100	(cm/s)**2
MERIDIONAL DRIFT	NAVY	(30°S, 180°E)	(0°N, 280°E)	250	±	75	(cm/s)**2
MERIDIONAL DRIFT	NAVY	(30°S, 280°E)	(0°N, 360°E)	150	±	50	(cm/s)**2
ZONAL DRIFT	NAVY	(0°N, 0°E)	(60°N, 100°E)	150	±	75	(cm/s)**2
ZONAL DRIFT	NAVY	(0°N, 100°E)	(60°N, 180°E)	250	±	100	(cm/s)**2
ZONAL DRIFT	NAVY	(0°N, 180°E)	(60°N, 280°E)	250	±	100	(cm/s)**2
ZONAL DRIFT	NAVY	(0°N, 280°E)	(60°N, 360°E)	250	±	100	(cm/s)**2
MERIDIONAL DRIFT	NAVY	(0°N, 360°E)	(60°N, 100°E)	150	±	150	(cm/s)**2
MERIDIONAL DRIFT	NAVY	(0°N, 100°E)	(60°N, 180°E)	200	±	100	(cm/s)**2
MERIDIONAL DRIFT	NAVY	(0°N, 180°E)	(60°N, 280°E)	275	±	75	(cm/s)**2
MERIDIONAL DRIFT	NAVY	(0°N, 280°E)	(60°N, 360°E)	250	±	150	(cm/s)**2

TABLE IV. Estimated asymptotic value of variance of WOCE buoy pair drift differences in rectangular regions of the globe as the buoy pair separation decreases to zero. There is some tendency for the asymptotic buoy drift variance to increase northwards; The asymptotic variance of the WOCE buoy drift is 25% of the Navy buoy error variance.

PARAMETER NAME	DATASET	CORNERS OF RECTANGULAR REGION (LATITUDE,LONGITUDE)	(LATITUDE,LONGITUDE)	VARIANCE	±		UNITS
ZONAL DRIFT	WOCE	(30°S, 100°E)	(0°N, 180°E)	40	±	25	(cm/s)**2
ZONAL DRIFT	WOCE	(30°S, 180°E)	(0°N, 280°E)	40	±	30	(cm/s)**2
ZONAL DRIFT	WOCE	(30°S, 280°E)	(0°N, 360°E)	20	±	15	(cm/s)**2
MERIDIONAL DRIFT	WOCE	(30°S, 100°E)	(0°N, 180°E)	40	±	25	(cm/s)**2
MERIDIONAL DRIFT	WOCE	(30°S, 180°E)	(0°N, 280°E)	20	±	30	(cm/s)**2
MERIDIONAL DRIFT	WOCE	(30°S, 280°E)	(0°N, 360°E)	20	±	15	(cm/s)**2
ZONAL DRIFT	WOCE	(0°N, 100°E)	(60°N, 180°E)	40	±	25	(cm/s)**2
ZONAL DRIFT	WOCE	(0°N, 180°E)	(60°N, 280°E)	40	±	30	(cm/s)**2
ZONAL DRIFT	WOCE	(0°N, 280°E)	(60°N, 360°E)	40	±	15	(cm/s)**2
MERIDIONAL DRIFT	WOCE	(0°N, 100°E)	(60°N, 180°E)	40	±	25	(cm/s)**2
MERIDIONAL DRIFT	WOCE	(0°N, 180°E)	(60°N, 280°E)	40	±	25	(cm/s)**2
MERIDIONAL DRIFT	WOCE	(0°N, 280°E)	(60°N, 360°E)	40	±	15	(cm/s)**2

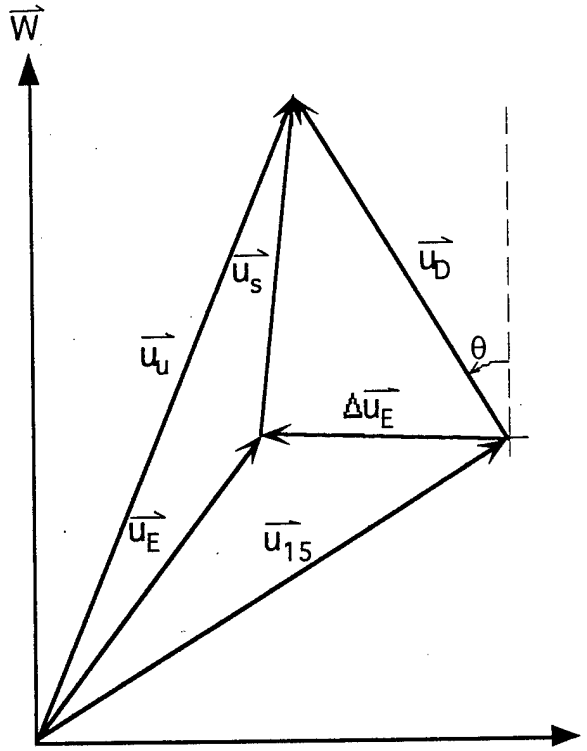

Figure 1. Undrogued buoy drift, u_u, and drogued buoy drift at 15 m. depth, u_{15}, relative to the wind vector, W. The deviant buoy drift vector, u_D, is the vector difference $u_{15} - u_u$. The undrogued buoy drift vector is the vector sum of the Ekman drift, u_E, and the slip, u_s. θ is the deviant drift response angle with respect to the wind.

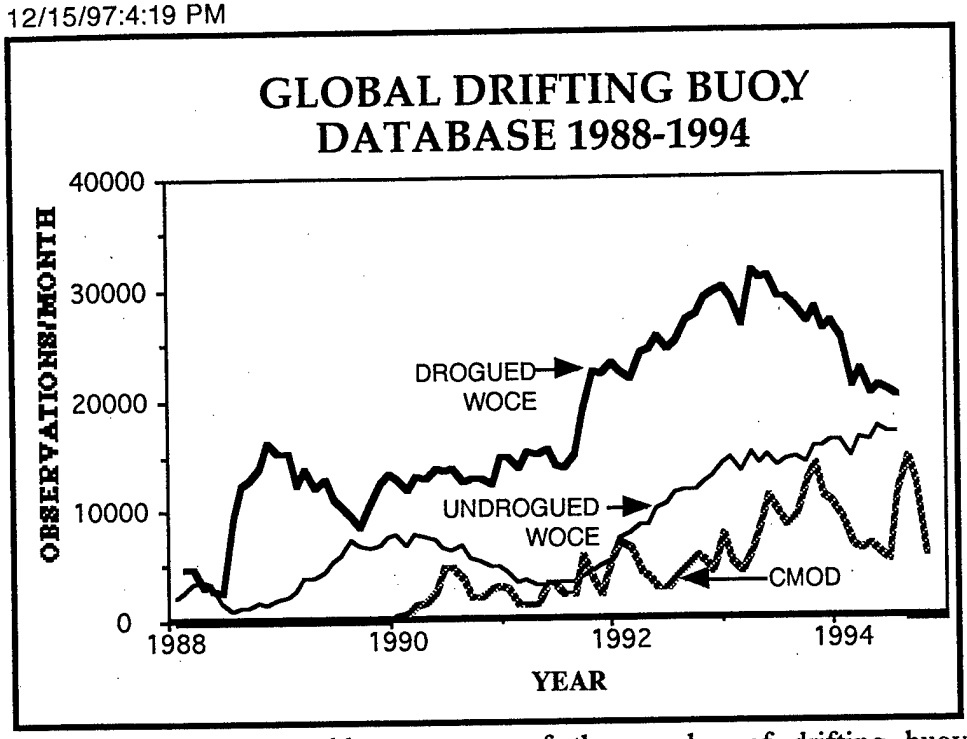

Figure 2. Global monthly summary of the number of drifting buoy observations per month in the Ocean Prospects data archive. The two WOCE/TOGA datasets are comprised of Lagrangian drifters deployed by the WOCE/TOGA scientific programs. Observations from a Lagrangian drifter are counted among the undrogued WOCE drifters after an on-board sensor indicates the buoy's drogue has been lost. The CMOD dataset is comprised of AN/WSQ-6 drifters deployed by the Navy.

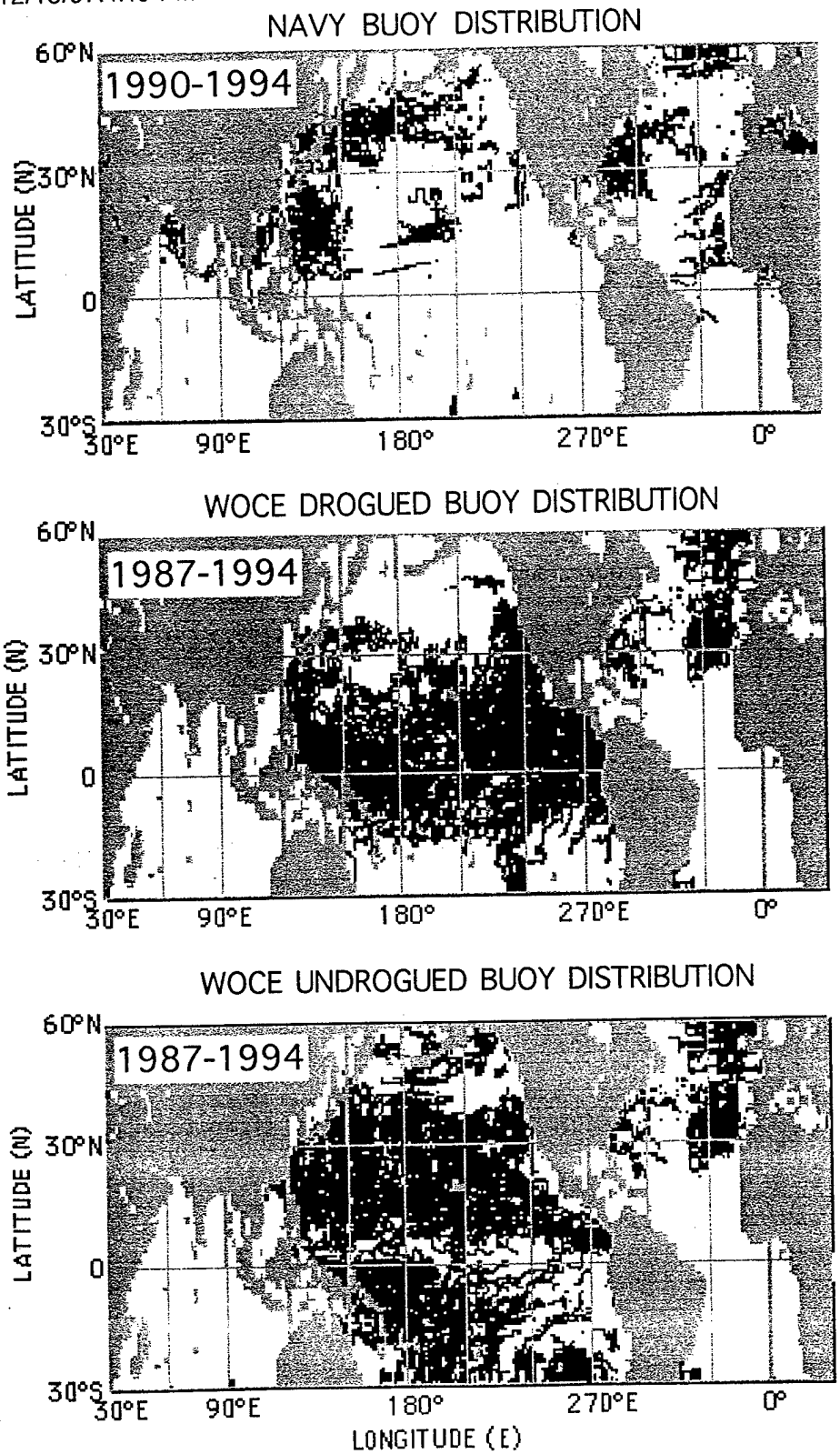

Figure 3. Global distribution of Navy (top) buoys for 1990-1994, WOCE drogued (middle) and WOCE undrogued (bottom) for 1988-1994.

A COMPARISON OF ECMWF AND FNMOC MEAN WINDS

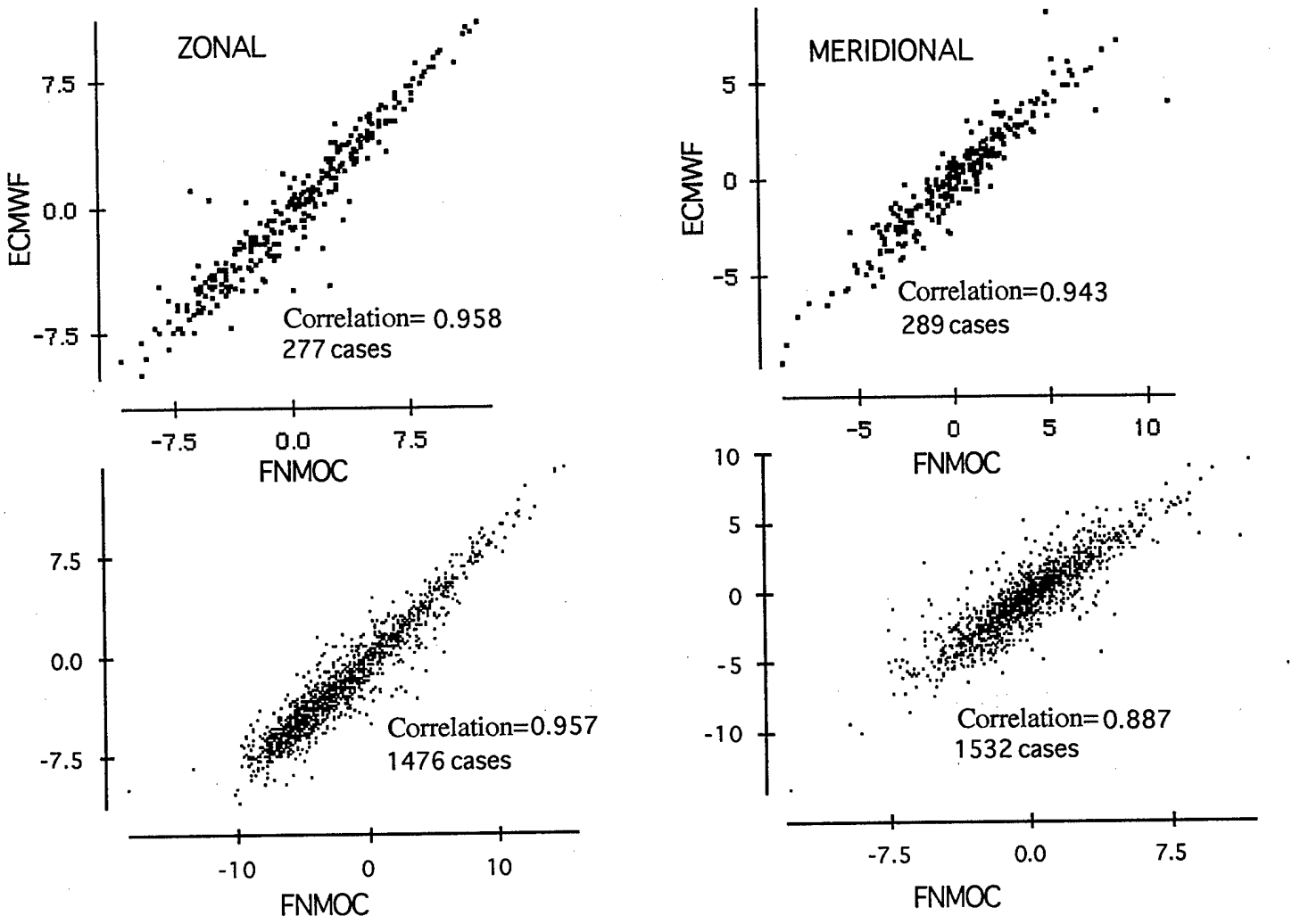

Figure 4. Scatterplots of interpolated Fleet Numerical Meteorology and Oceanography Central (FNMOC) winds vs. interpolated European Center for Medium-Range Forecasting (ECMWF) winds were made for the WOCE/TOGA drogue-on/drogue-off dataset (bottom) and the WOCE/TOGA drogue-on/Navy dataset (top).

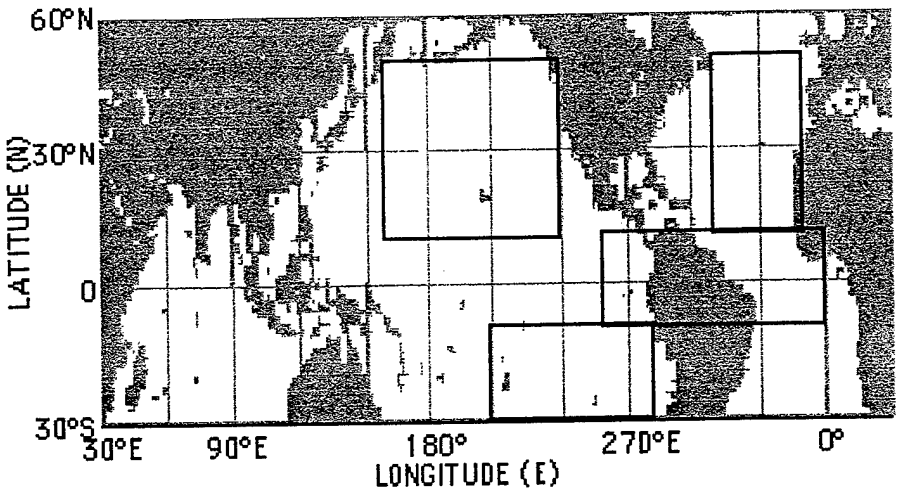

Figure 5. The four regions selected for relatively low wind speed variability and wave height variability. Climatological horizontal shear in the upper ocean was low and observational density was relatively high in these regions, with the exception of the equatorial box, which was chosen to provide some insight into processes near the equator.See discussion in text.

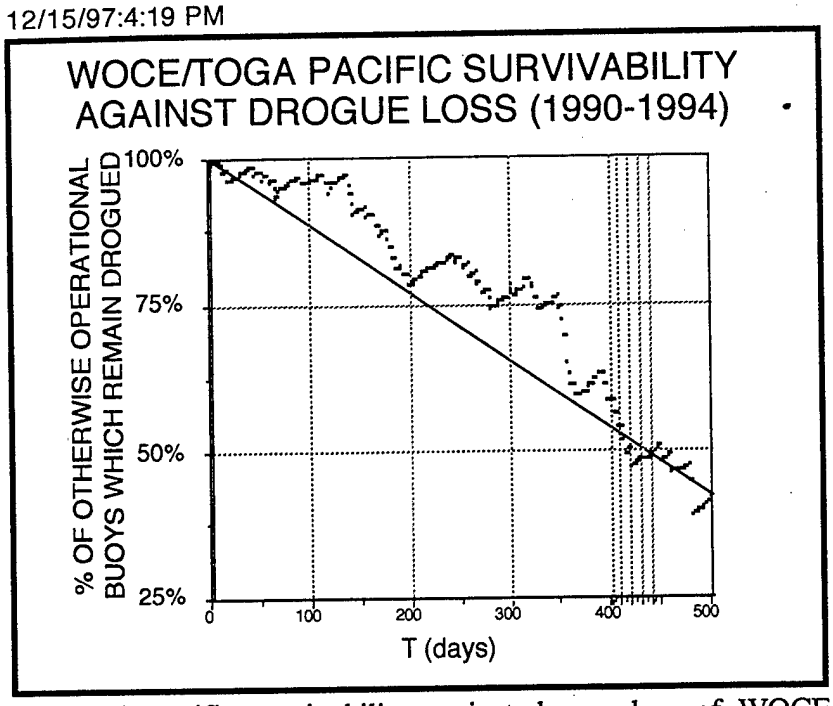

Figure 6. Pacific survivability against drogue loss of WOCE buoy data from 1990-1994; duration, T, is the number of datays since deployment. Since the percent of surviving drogued buoys has been normalized to the number of buoys, drogued or undrogued, which have survived, it is possible for the survivability to occasionally increase. The straight line shows the number of drogued buoys predicted by a simple linear model of drogue survivability.

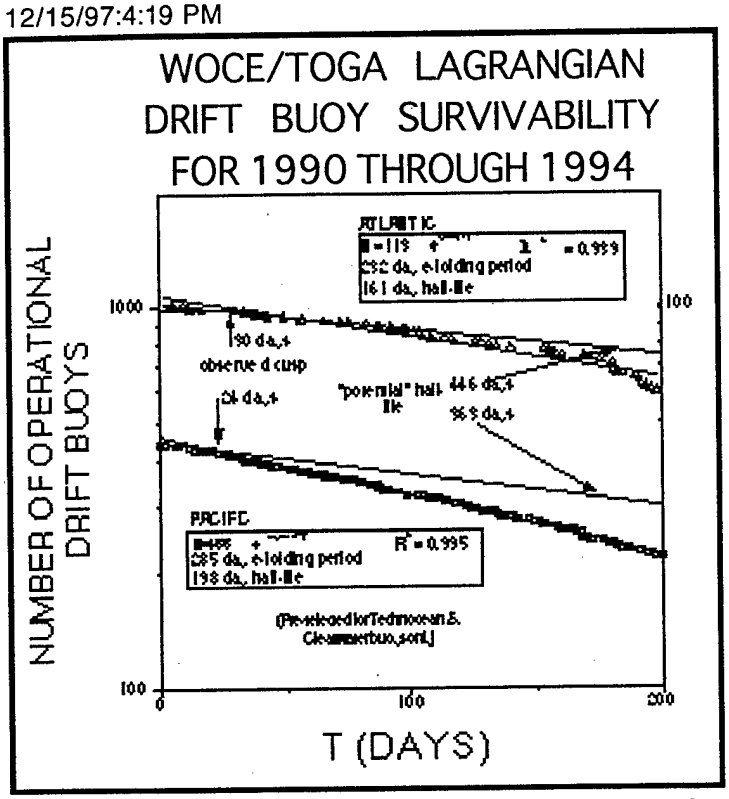

Figure 7. Global survivability to all causes other than drogue loss of WOCE/TOGA Lagrangian drift buoys for deployments during the period 1990-1994; duration, T, is the number of days since deployment.

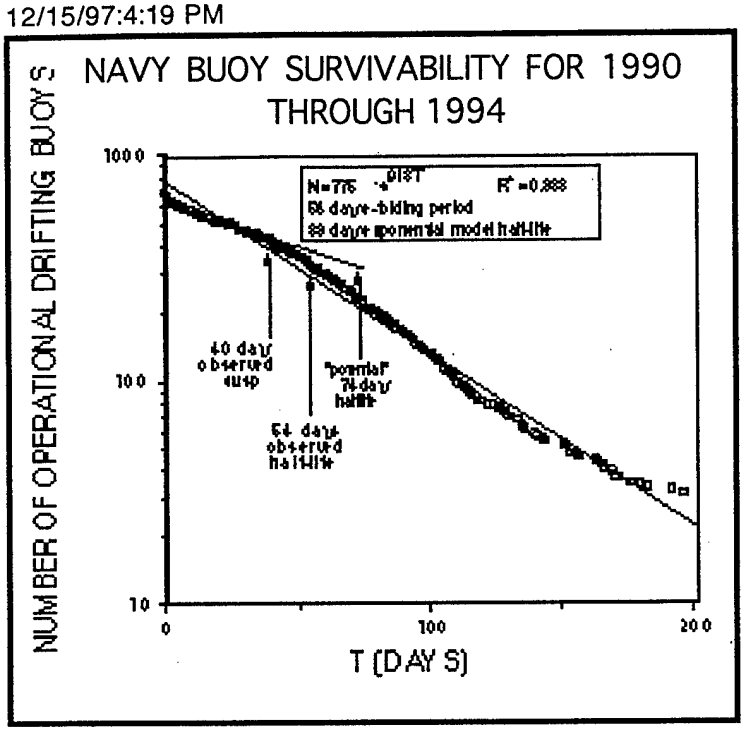

Figure 8. Global survivability against all causes of failure other than drogue loss of AN/WSQ-6 buoys for deployments during the period 1990-1994; duration, T, is the number of days since deployment. The heavy straight line is the expected population of surviving drift buoys predicted by an exponential model; the light straight line is the expected population of surviving drift buoys predicted by an exponential model based upon the first 40 days of data.

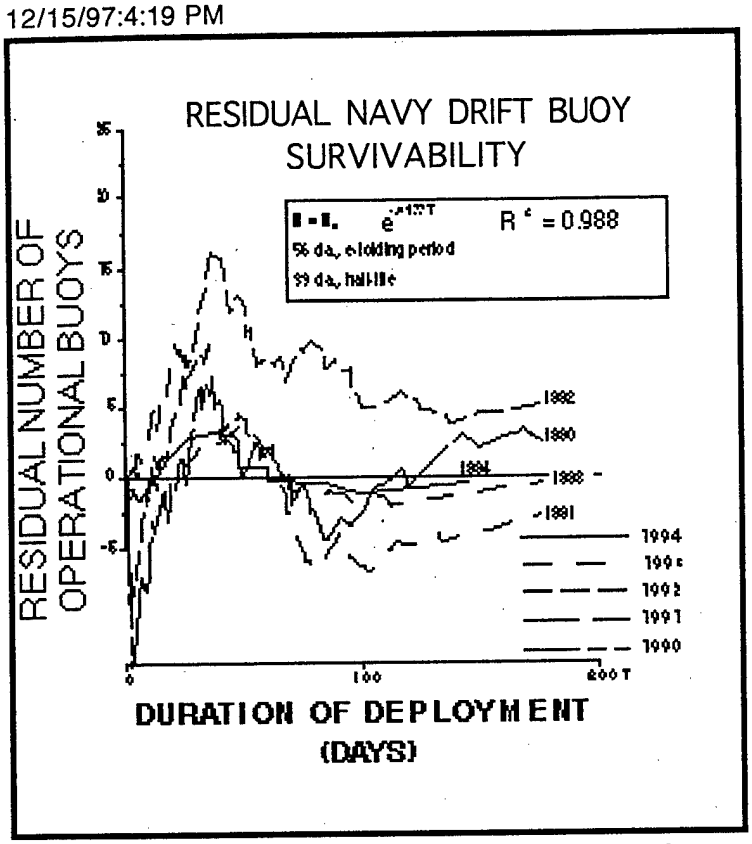

Figure 9. The residual number of operating buoys, drogued or undrogued which remain after subtracting the number expected from the exponential model. The analysis was made for Navy drifting buoys deployed during each of the years 1990, 1991, 1992, 1993, and 1994; N_0 is the total number of buoys deployed in each year. The residual number peaks between 30 days and 50 days, implying a great increase in the buoy failure rate at this time.

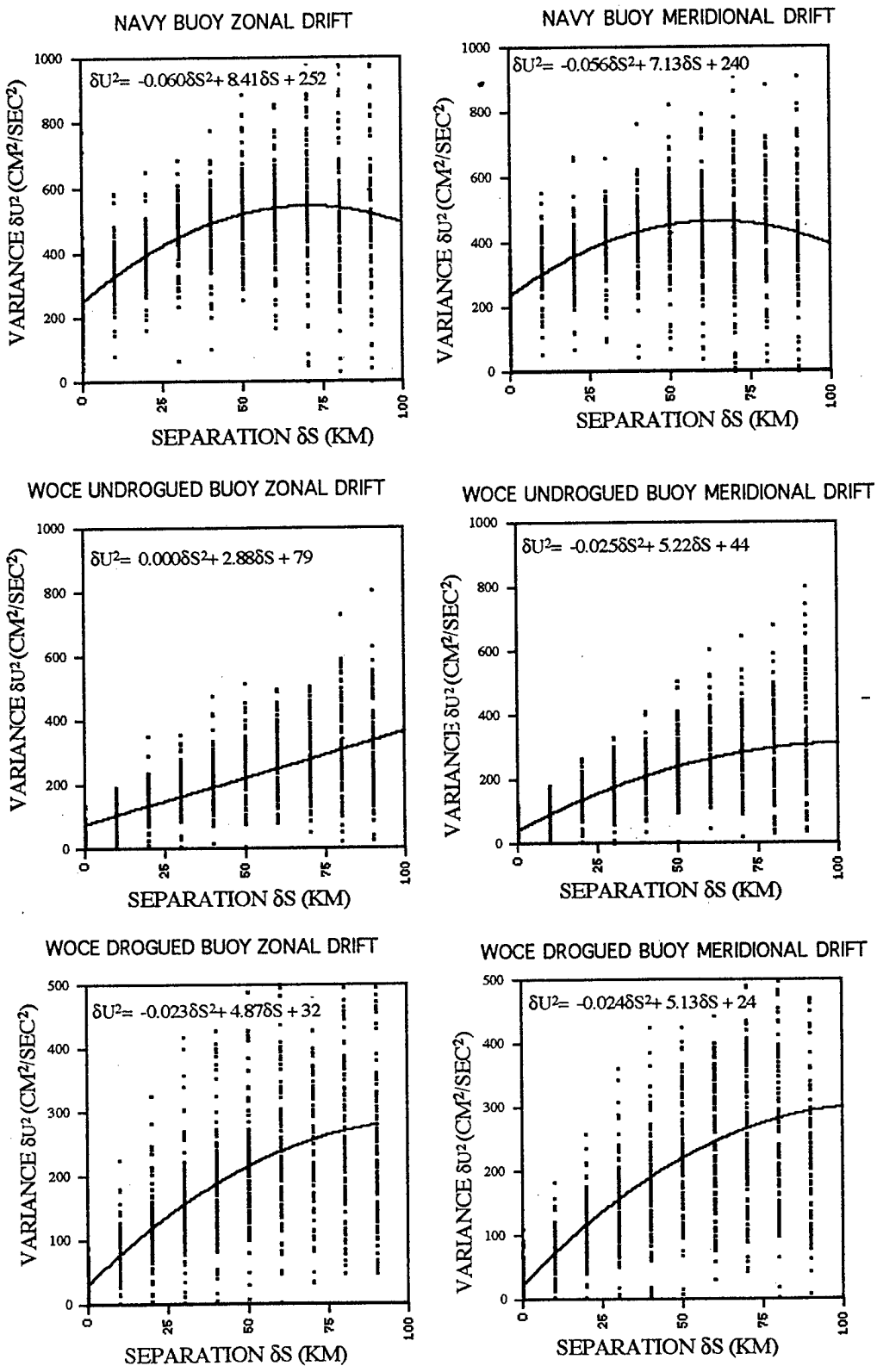

Figure 10. The variance of buoy drift zonal (left) and meridional (right) velocity components versus separation. A least-squares fit to a quadratic equation yields the intercept at no separation for (TOP) Navy buoys; (MIDDLE) WOCE undrogued buoys; (BOTTOM) WOCE drogued buoys. The Navy buoy intercept is larger than the WOCE buoy intercept, not because of any inherent defect in the buoy, but because of differences in the way they are tracked and their position transmitted.

PROBABILITY DISTRIBUTION OF NAVY BUOY DEVIATION RESIDUALS FROM MODEL

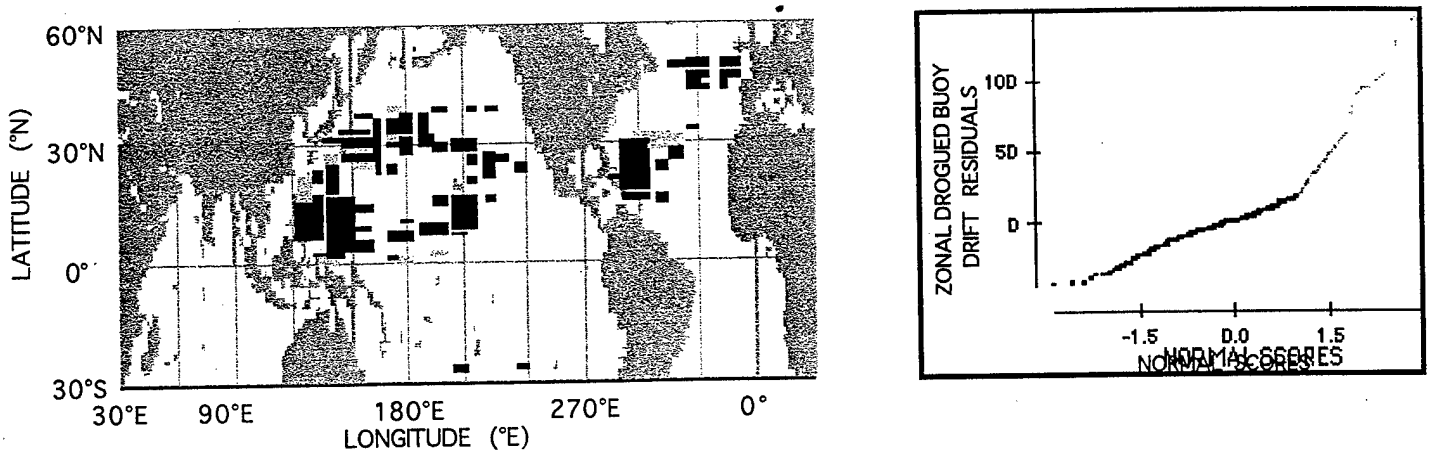

PROBABILITY DISTRIBUTION OF WOCE BUOY DEVIATION RESIDUALS FROM MODEL

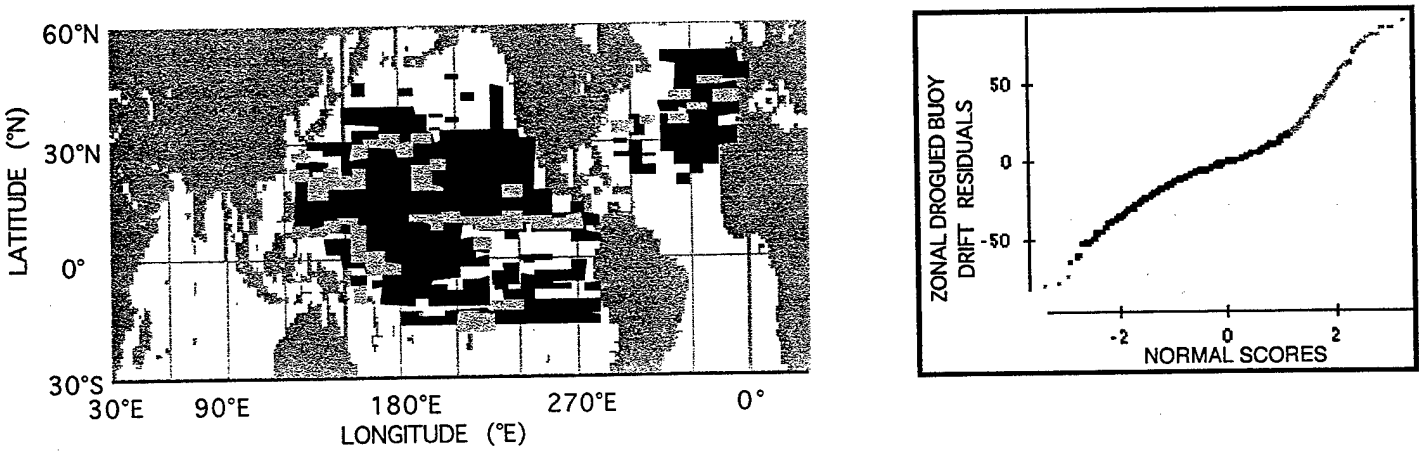

Figure 11. (Top) The graph of residuals vs. the normal score statistic is a straight line if the assumption that the distribution of residuals from the regression are normal is true. (Bottom) Spatial distribution of 2° latitude by 8° longitude by 1 month summaries used in the regression analysis. Light shades denote regions where an anomalous relationship holds between wind and zonal drogued buoy drift velocity.

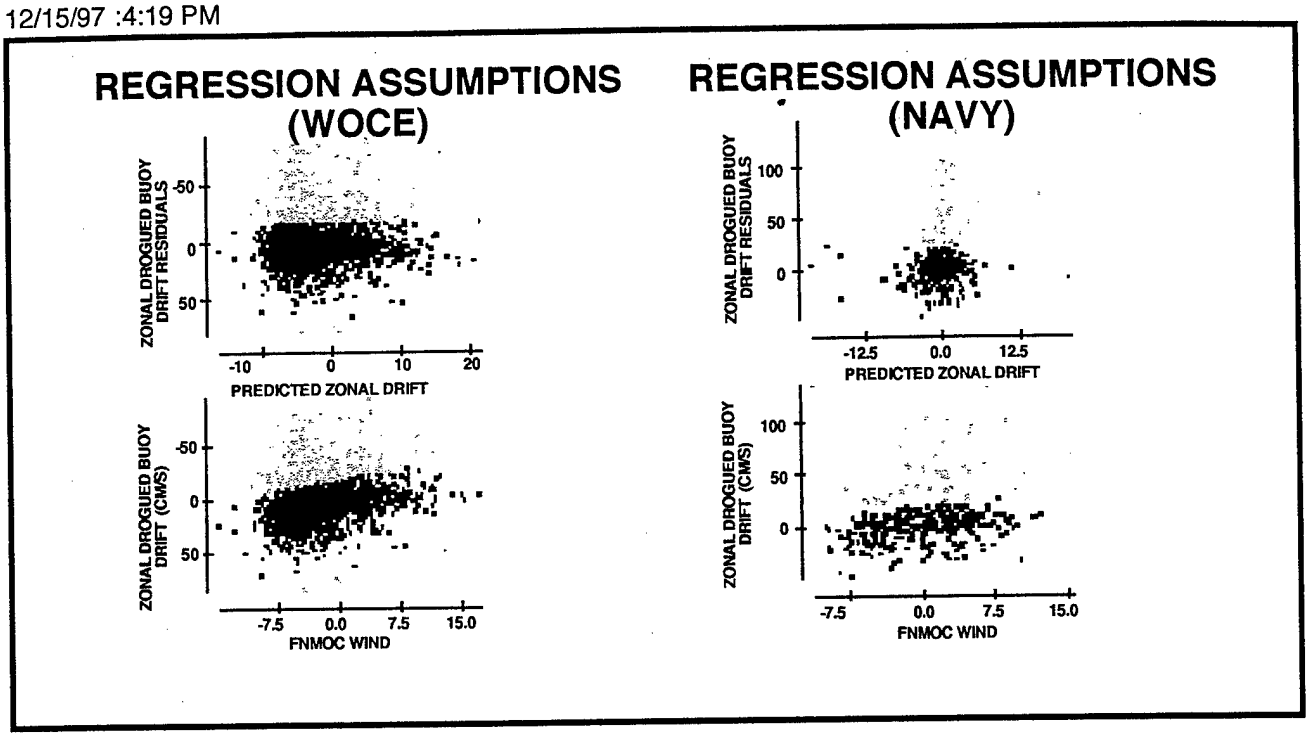

Figure 12. (TOP) A monotonically increasing or decreasing trend in residuals vs. the predicted drift would violate the assumption that residuals have constant variance. (BOTTOM) The linear trend with increasing wind velocity is visible but noisy in these unselected and unedited scatterplots. The gray shaded points are data with an anomalous probability distribution (see previous figure).

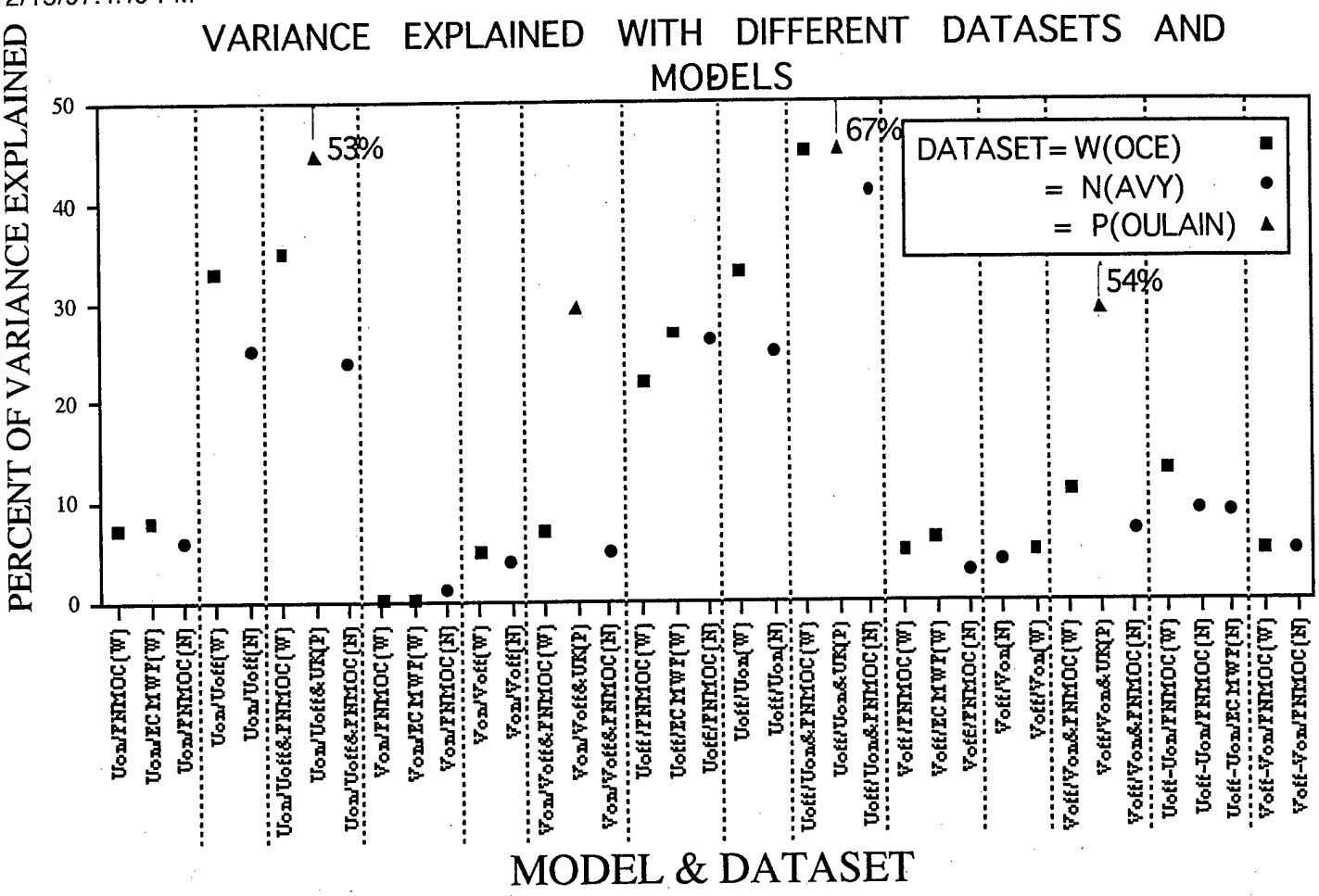

Figure 13. Dashed bars separate different models. Each model is a regression of a dependent variable, y, upon one or more predictors, x or w, x and y are either drogued or undrogued buoy zonal (meridional) velocity and w is zonal (meridional) wind velocity drawn from one of three datasets. The vertical labels code this information into a single line: DEPENDENT/PREDICTOR (DATASET). For instance, the leftmost label is "Uon/FNMOC (W)," meaning the dependent variable, y is Uon (drogued buoy zonal velocity, the buoy drift velocity predictor, x, is undefined, the wind velocity predictor, w, is FNMOC zonal wind velocity, and the dataset is the WOCE/TOGA drogue on vs. drogue off.

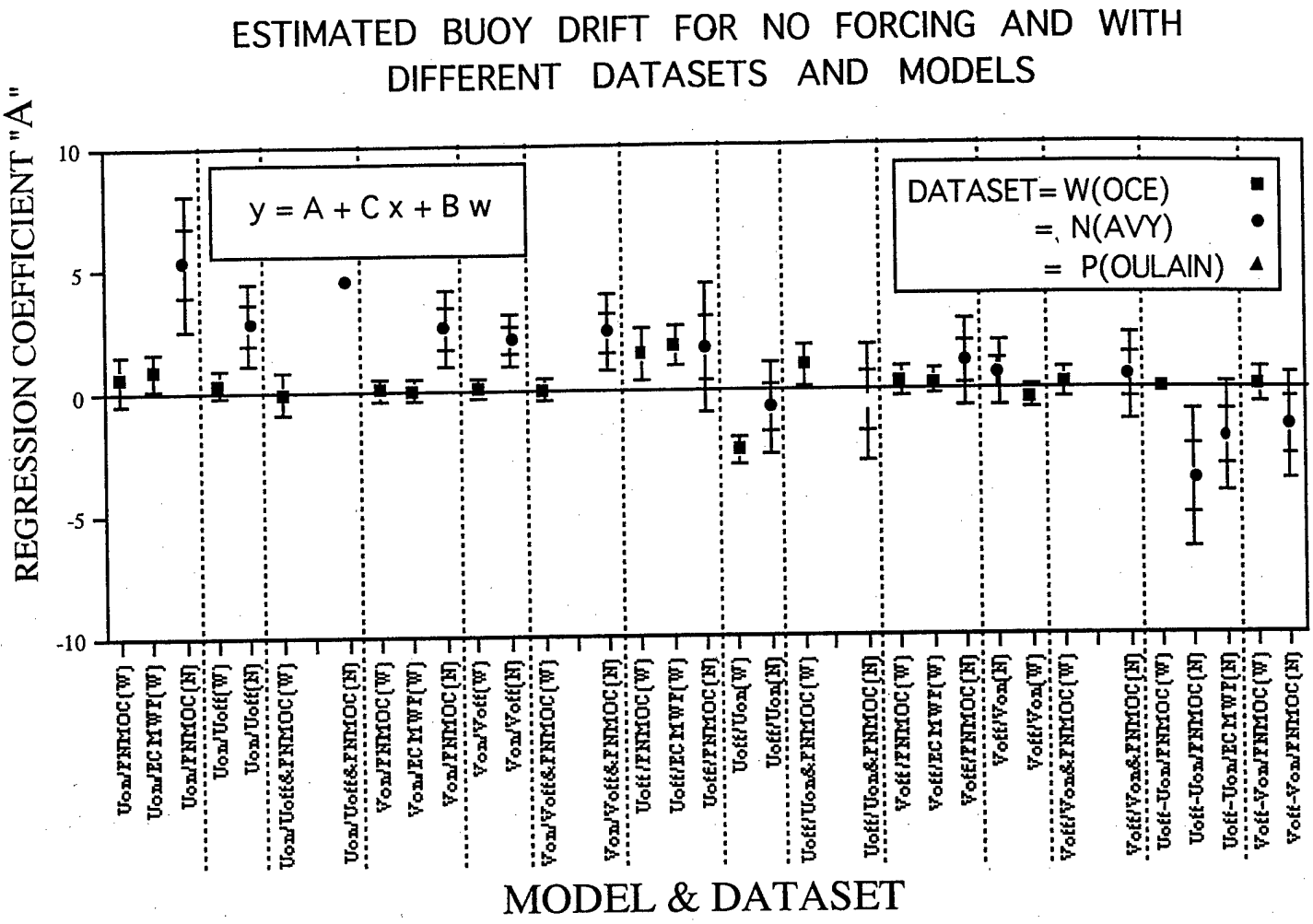

FIGURE 14. Dashed bars separate different models. Each model is a regression of a dependent variable, y, upon one or more predictors, x or w; x and y are either drogued or undrogued buoy zonal (meridional) velocity and w is zonal (meridional) wind velocity drawn from one of three datasets. The vertical labels code this information into a single line: DEPENDENT/PREDICTOR(DATASET). For instance, the leftmost label is "Uon/FNMOC(W)," meaning the dependent variable, y, is Uon (drogued buoy zonal velocity), the buoy drift velocity predictor, x, is undefined, the wind velocity predictor, w, is FNMOC zonal wind velocity, and the dataset is the WOCE/TOGA, drogue on vs. drogue off. Error bars are the 95% confidence interval of the mean value of "A"; error bars are not shown where their length is same order as the symbol size.

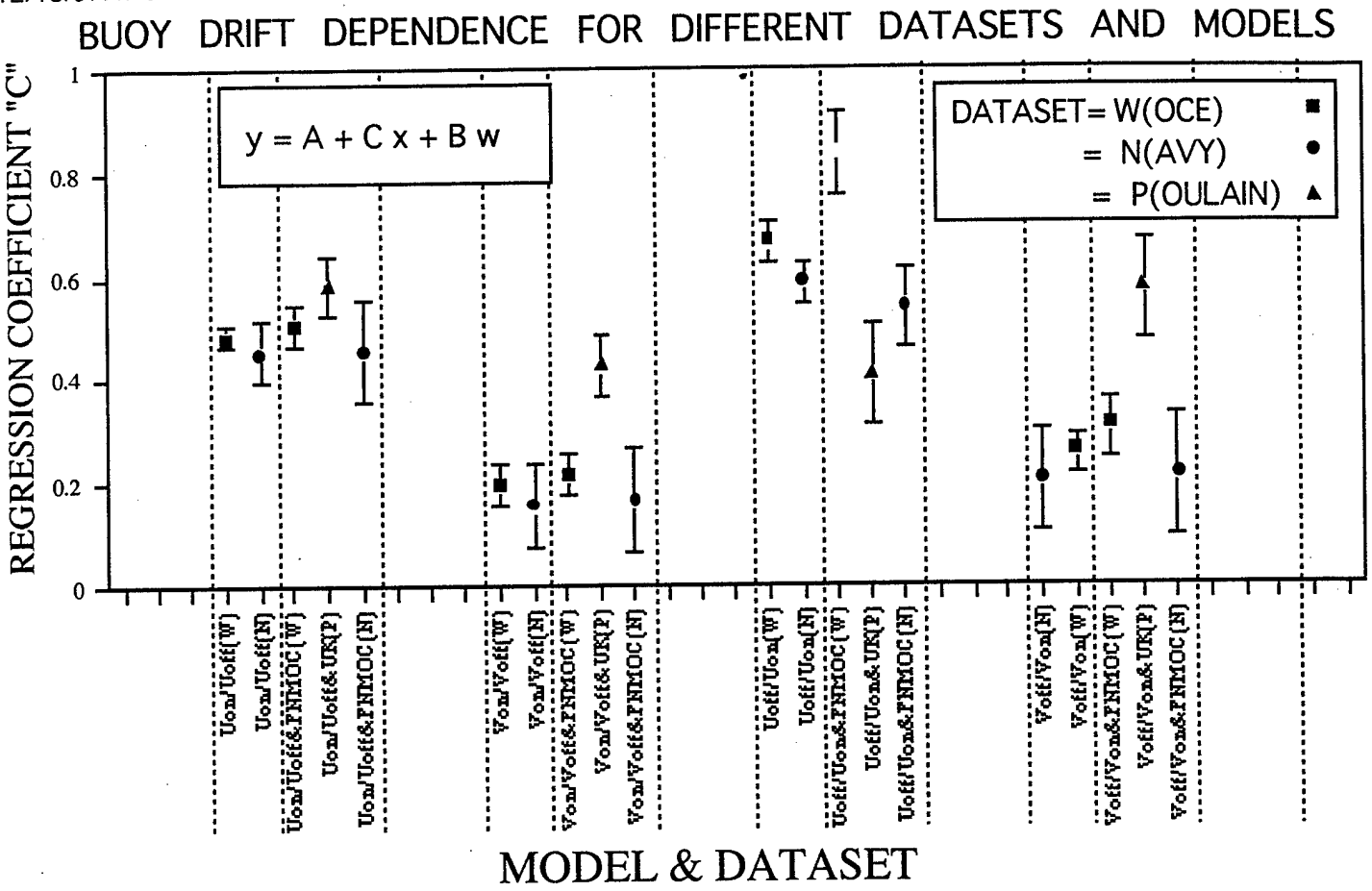

Figure 15. Dashed bars separate different models. Each model is a regression of a dependent variable, y, upon one or more predictors, x or w, x and y are either drogued or undrogued buoy zonal (meridional) velocity and w is zonal (meridional) wind velocity drawn from one of three datasets. The vertical labels code this information into a single line: DEPENDENT/PREDICTOR (DATASET). For instance, the leftmost label is "Uon/FNMOC (W)," meaning the dependent variable, y is Uon (drogued buoy zonal velocity, the buoy drift velocity predictor, x, is undefined, the wind velocity predictor, w, is FNMOC zonal wind velocity, and the dataset is the WOCE/TOGA drogue on vs. drogue off. Error bars are the 95% confidence interval of the mean value of "C," error bars are not shown where their length is the same order as the symbol size. No values are plotted where the model postulates no dependence on buoy drift velocity.

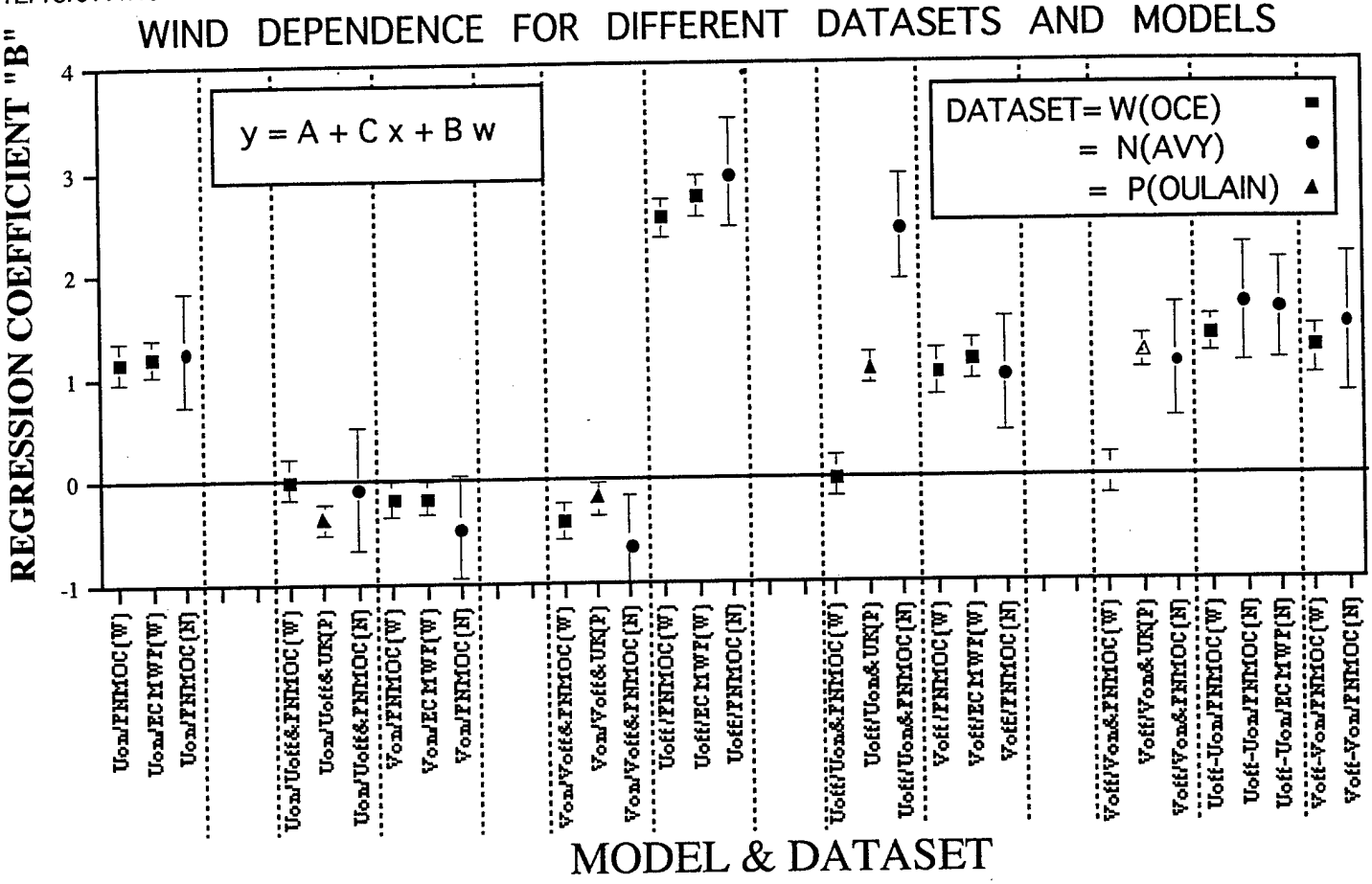

Figure 16. Dashed bars separate different models. Each model is a regression of a dependent variable, y, upon one or more predictors, x or w, x and y are either drogued or undrogued buoy zonal (meridional) velocity and w is zonal (meridional) wind velocity drawn from one of three datasets. The vertical labels code this information into a single line: DEPENDENT/PREDICTOR (DATASET). For instance, the leftmost label is "U_{on}/FNMOC (W)," meaning the dependent variable, y is U_{on} (drogued buoy zonal velocity, the buoy drift velocity predictor, x, is undefined, the wind velocity predictor, w, is FNMOC zonal wind velocity, and the dataset is the WOCE/TOGA drogue on vs. drogue off. Error bars are the 95% confidence interval of the mean value of "B," error bars are not shown where their length is the same order as the symbol size. No values are plotted where the model postulates no dependence on wind velocity.

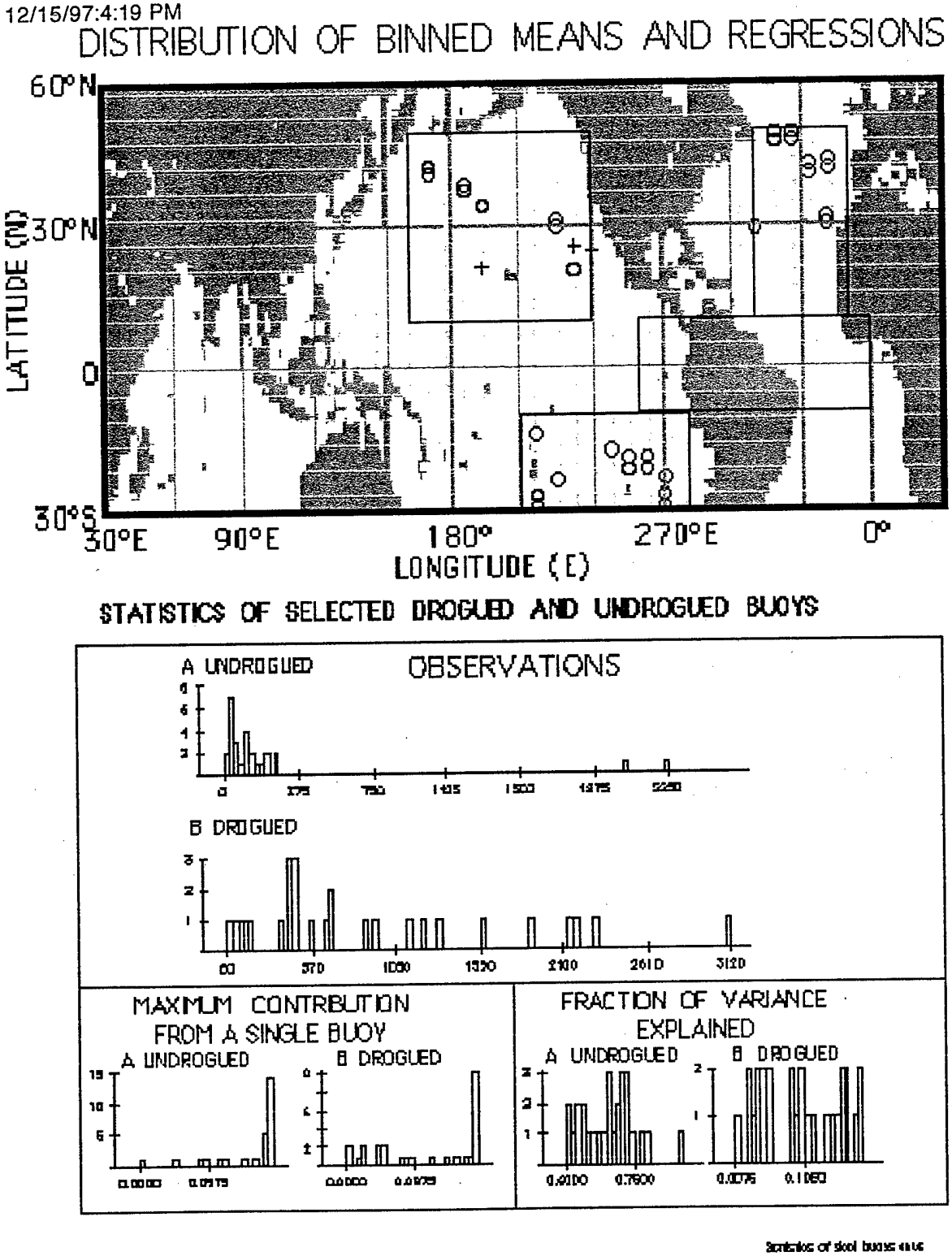

Figure 17. (TOP) Distribution of binned means and regressions where both undrogued (Navy) buoy data and drogued buoy data exists in a single 2° latitude by 8° longitude bin; selected bins are black circles (WOCE) and crosses (NAVY); (BOTTOM) Histogram of the number of buoy observations per selected bin; (BOTTOM LEFT) Histogram of the maximum percent of observations contributed by a single buoy to a mean undrogued buoy statistic in selected bins; (BOTTOM RIGHT) Histogram of the fraction of variance explained by a complex linear regression of buoy drift on wind in selected bins.

DEVIANT DRIFT SPEED VS. WIND SPEED

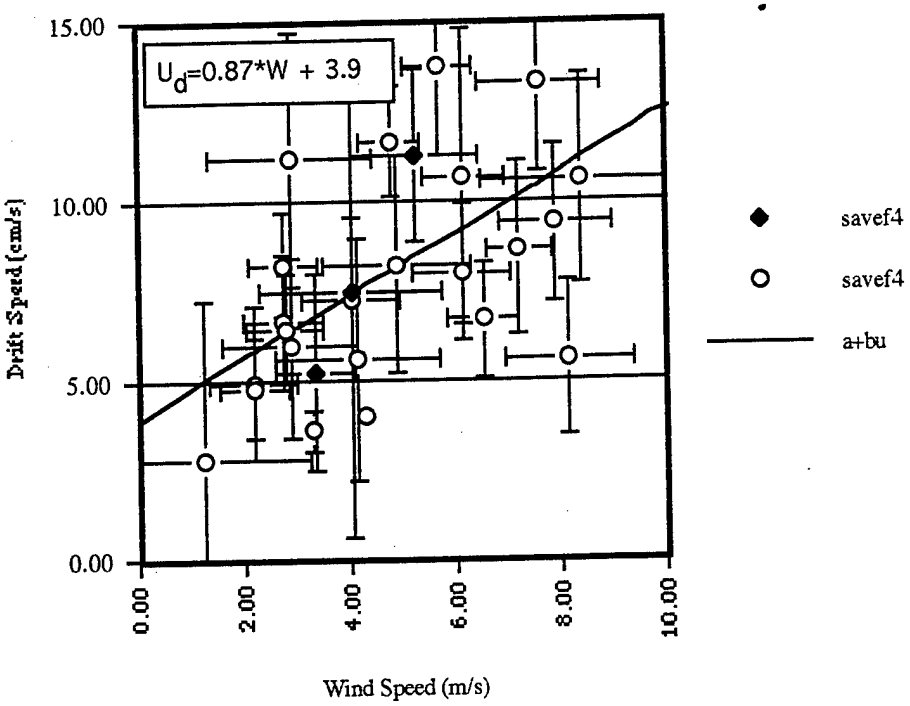

REGRESSION COEFFICIENT
VS.
LATITUDE

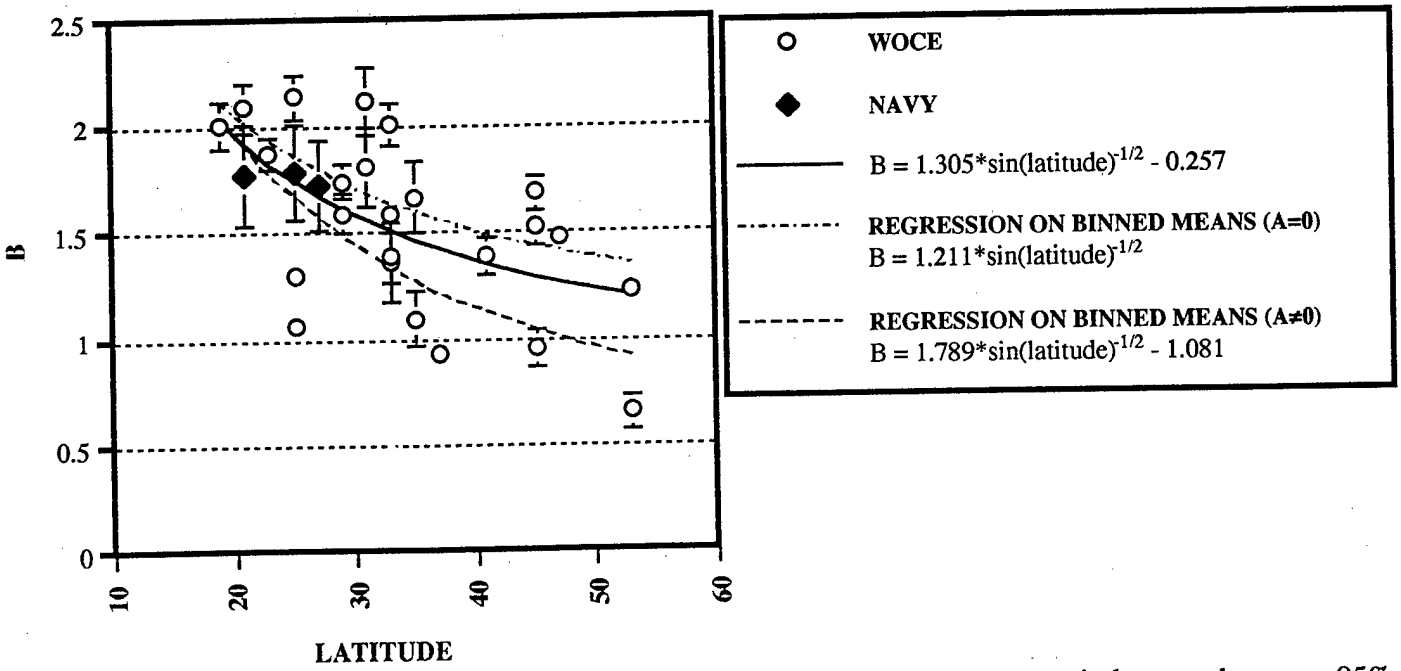

Figure 18 (TOP) WOCE (circle) and Navy (diamond) buoy drift deviation on wind; error bars are 95% confidence limits. (BOTTOM) WOCE (circle) and Navy (diamond) regression coefficients of vector buoy drift deviation on vector wind vs. latitude; error bars are 95% confidence limits. The model assumes an inverse square-root dependence upon the Coriolis parameter.

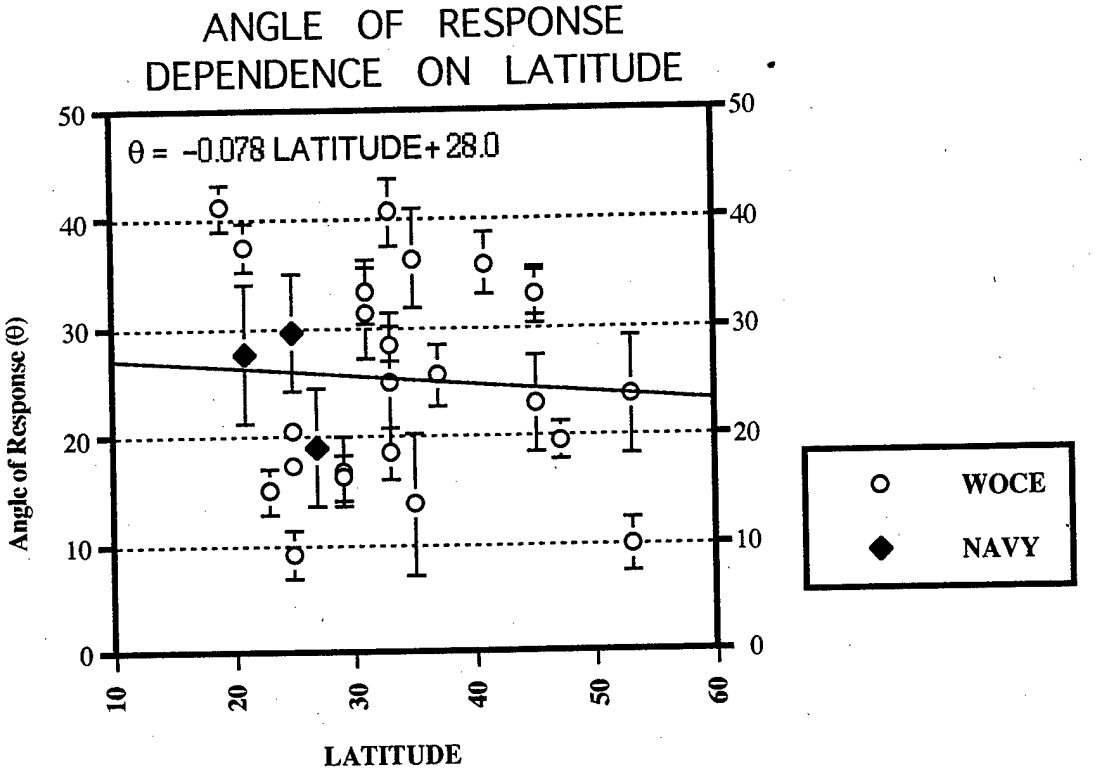

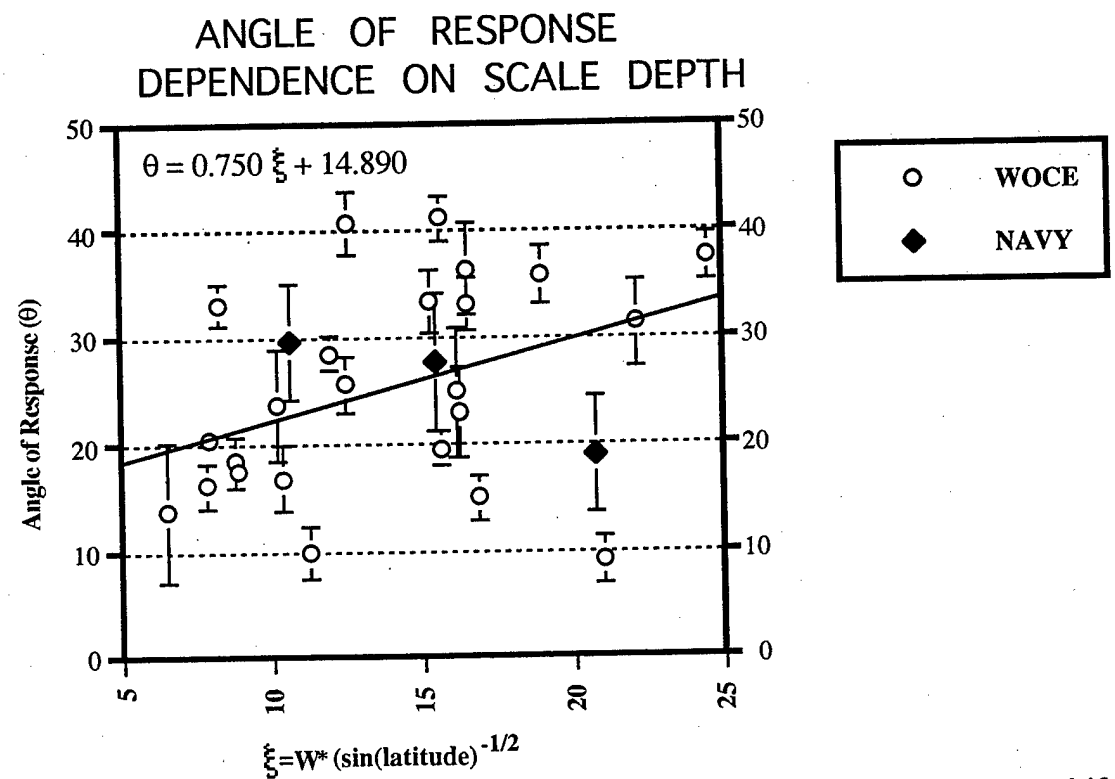

Figure 19. WOCE (circle) and Navy (diamond) angle of response of vector buoy drift deviation to vector wind vs. latitude; error bars are 95% confidence limits. The angle is left (right) of the wind in the northern (southern) hemisphere. There is no significant trend ofθ vs. latitude (top), but there is a significant trend ofθ vs. the scale depth ξ (bottom) with 98% confidence.

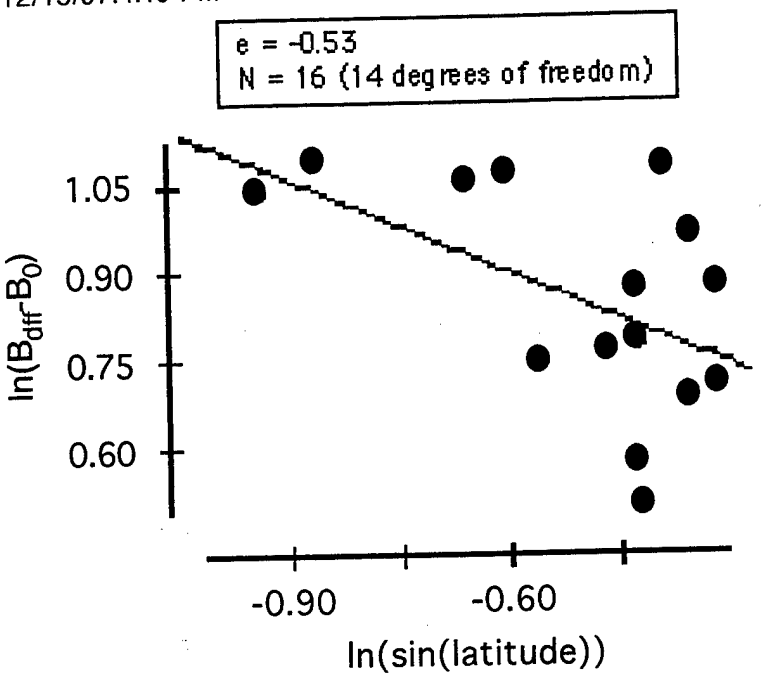

Figure 20. Given observed regression coefficients, B, of deviant drift on wind at different latitudes, the least-squares solution for the exponent of sin(latitude) is -0.53, supporting the choice of an exponent of -1/2 in the deviant drift model.

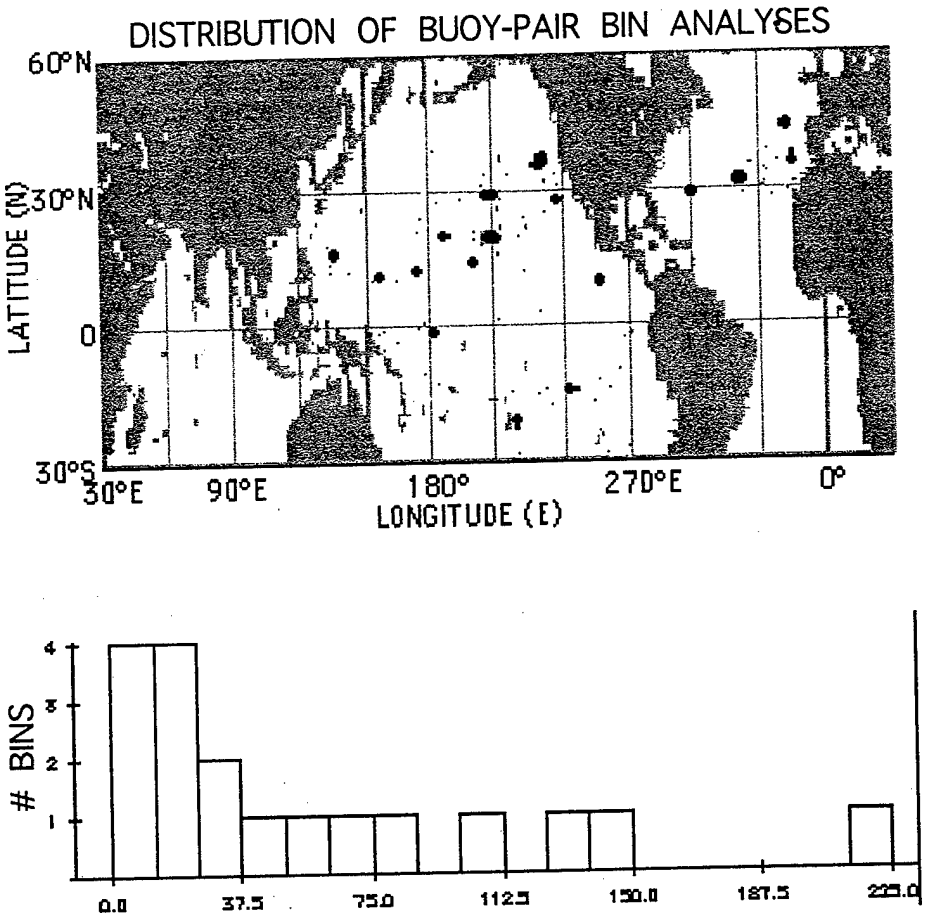

Figure 21. (TOP) Dark dots indicate the distribution of selected buoy-pair analyses; light shaded dots are not selected; (BOTTOM) Histogram of the number of observations in bins selected for buoy-pair analyses.

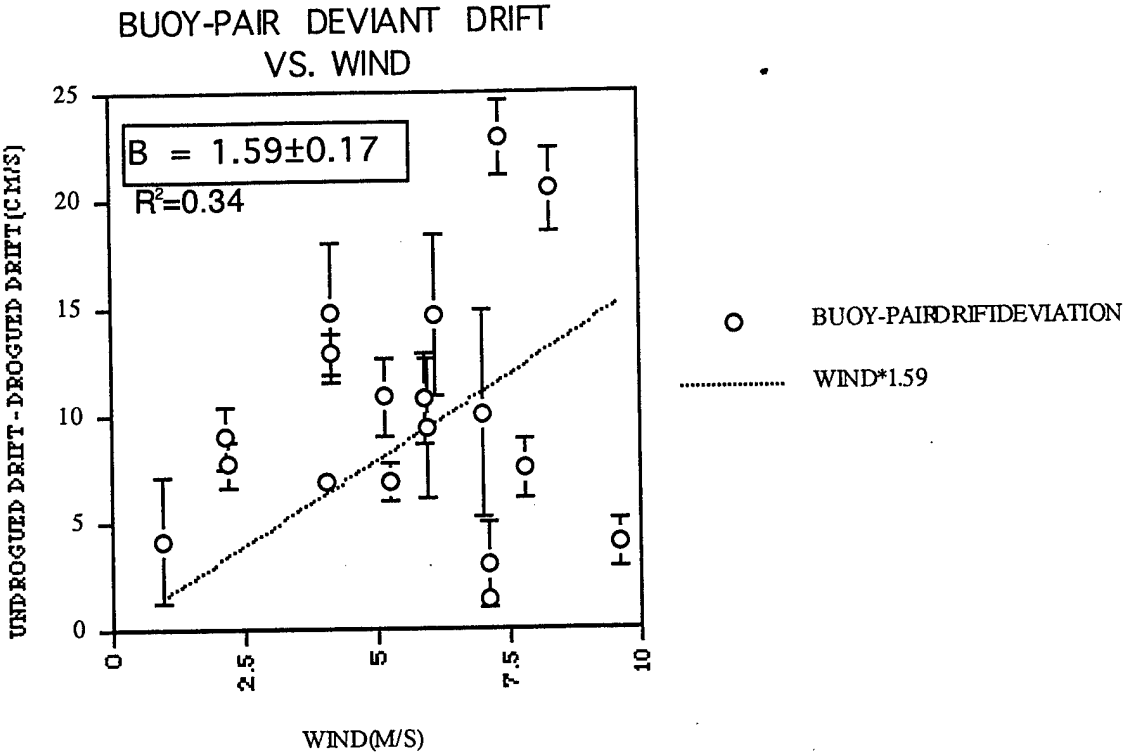

Figure 22. A scatterplot of selected buoy pair deviant drift vs. wind speed; 38 bins have been selected. The straight line explains 34% of the variance.

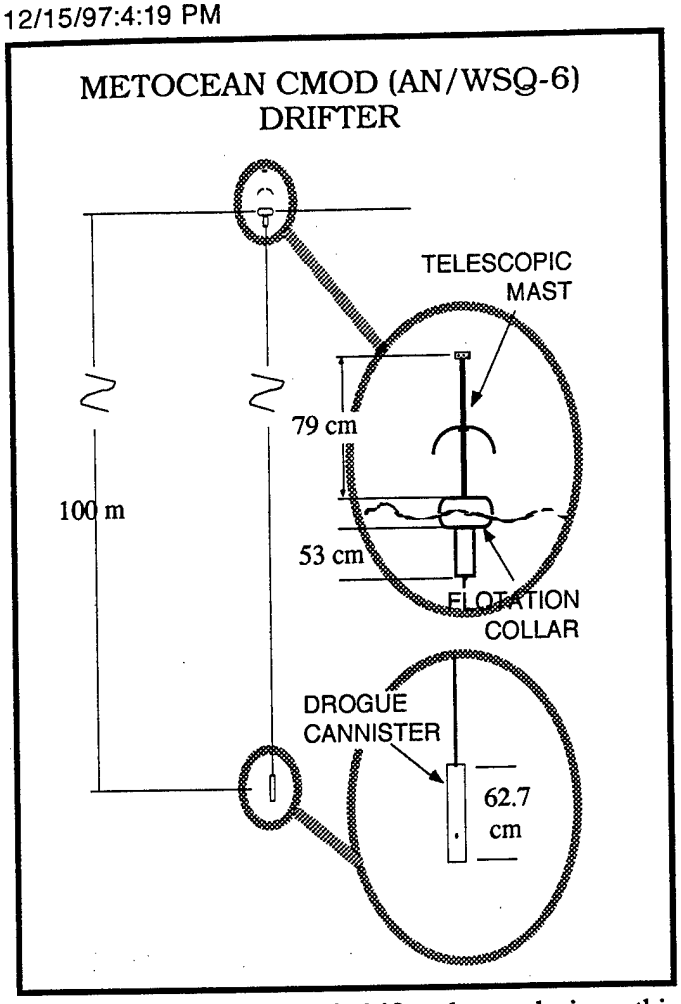

Figure A1.1 AN/WSQ-6 drifter buoy design; this schematic is after ARGOS 61532, deployed February 9, 1992. Its manufacturer's designation is CMOD I, a multi-parameter, satellite reporting mini buoy series for Tactical Oceanographic Warfare Support. (from METOCEAN Ltd.) CMOD II is much the same except for a larger flotation collar.

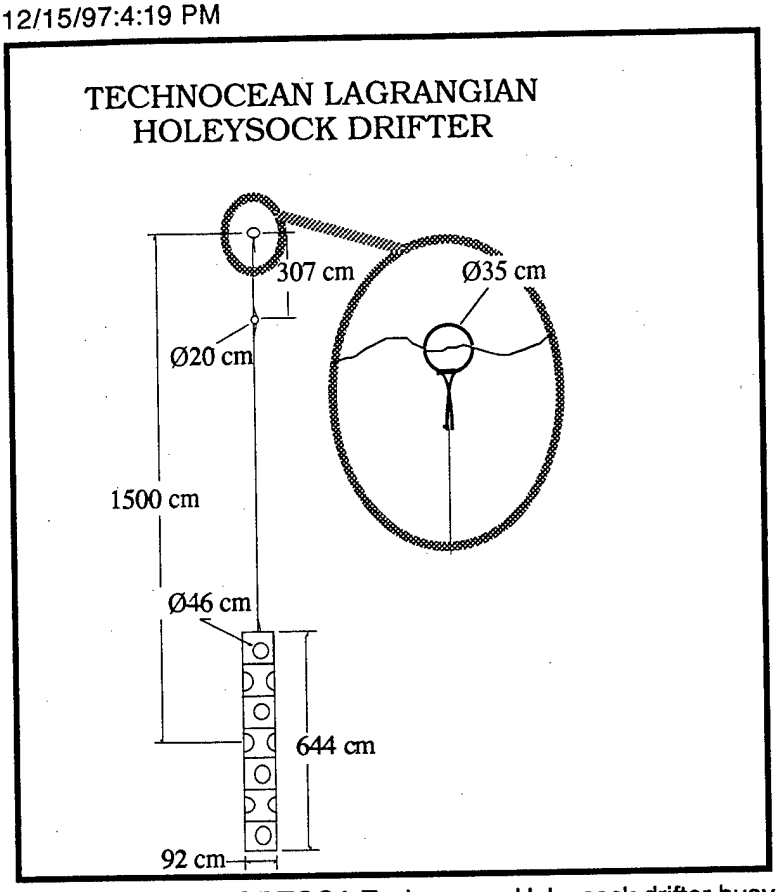

FIGURE A1.2 WOCE/TOGA Technocean Holeysock drifter buoy design; this is after ARGOS buoy 1425, deployed January 12, 1994. Note the enormous size of the drogue relative to that of the Metocean AN/WSQ-6 (CMOD) shown in Figure 4. It has a subsurface float and Urethane carrots at all float-tether connections mediating the stress on the tether. The exploded 4x view of the surface float is included in order to enable a better intercomparison with other buoy schematics.

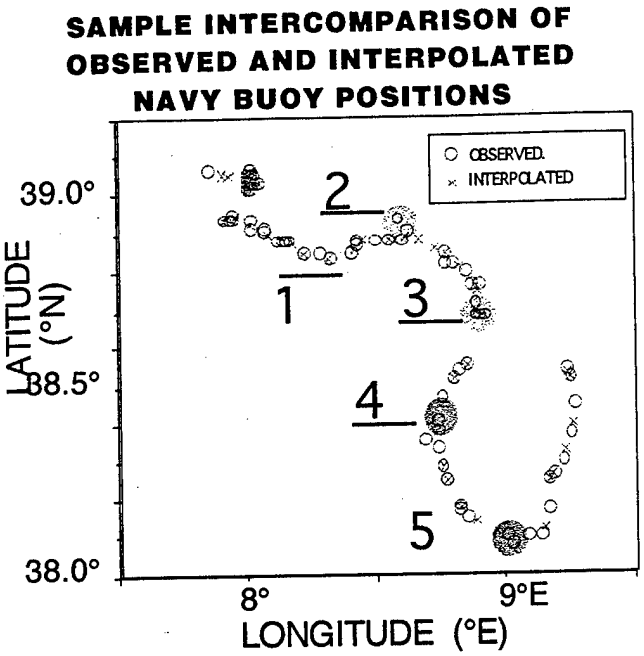

Figure D.1. Worm track of Navy AN/WSQ-6 buoy deployed during May, 1990. The numbered and shaded circles indicate times where it is difficult to calculate interpolated buoy drift velocities.

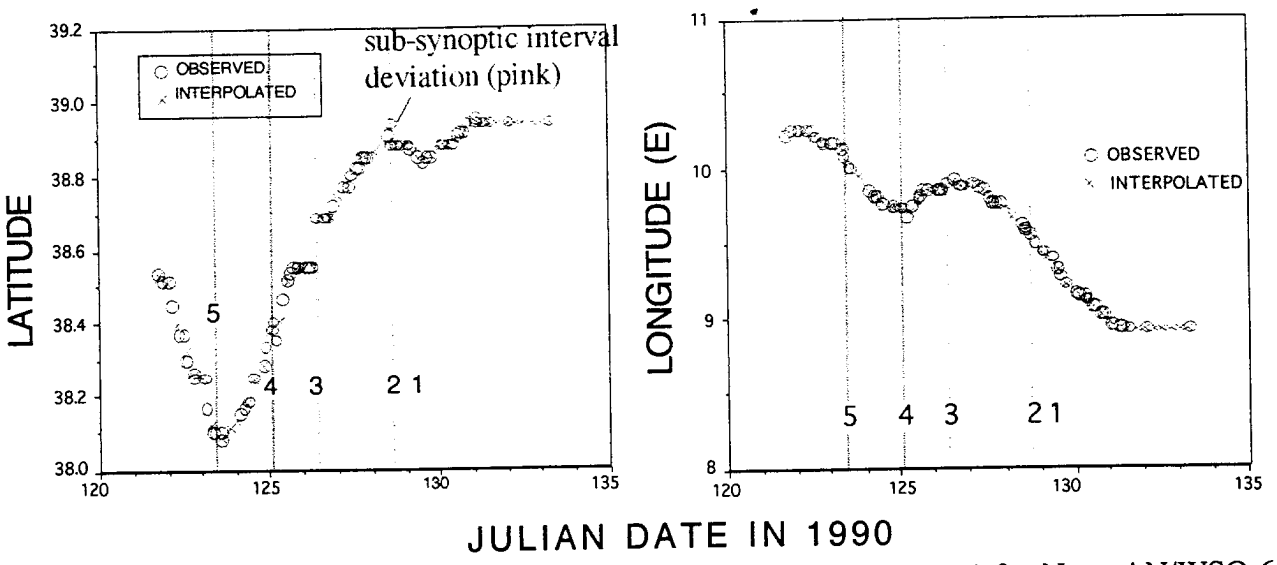

Figure D.2. Interpolated and observed latitudes (top) and longitudes (bottom) for Navy AN/WSQ-6 drift buoy 12501. Between 12 GMT and 18 GMT on day 128, the buoy "jogged" in its path; since this is less than a synoptic interval, the interpolation doesn't pick it up.

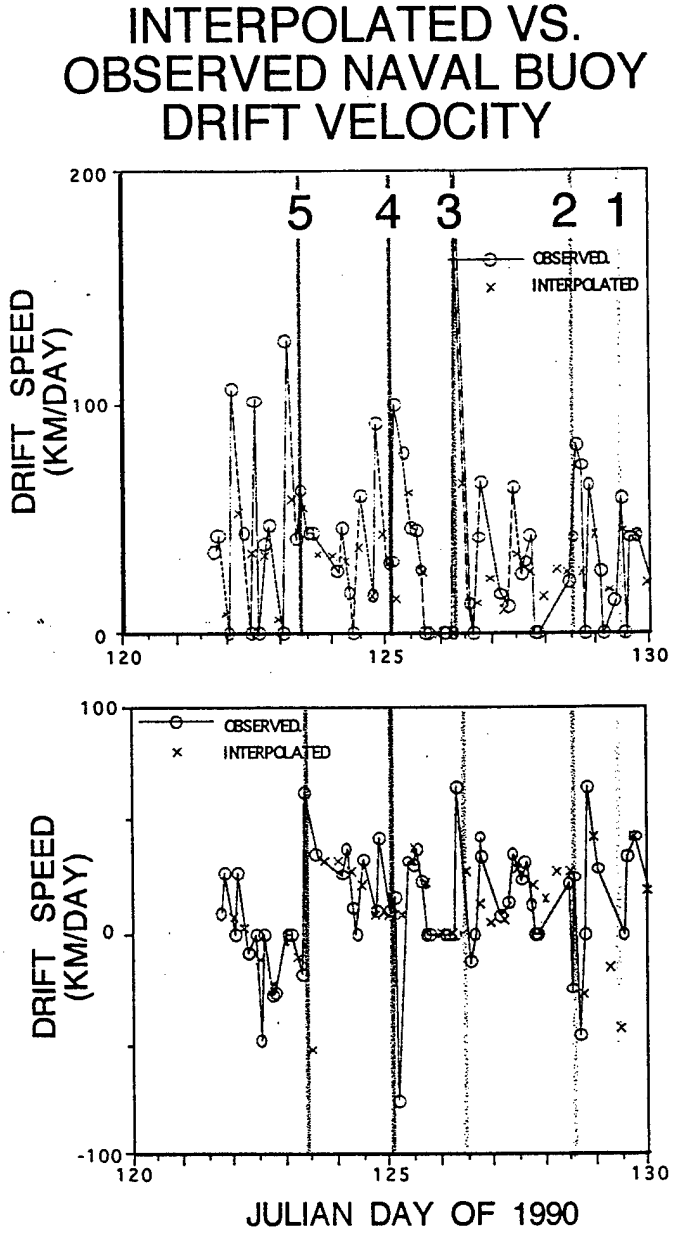

Figure D.3. Interpolated and observed meridional (top) and zonal (bottom) velocity components of Navy AN/WSQ-6 drift buoy 12501.

Ocean Prospects
204 N. El Camino Real, Suite 619
Encinitas, CA 92024

12/23/97

Mr. Edward C. Mozley
NRL,TOWS, Code 7406
Stennis Space Center, MS 39529-5004

Dear Mr. Mozley,

Enclosed you will find the final report for the contract N00014-95-C-6002. I am sending you all copies noted in the distribution list except the one reserved for the ACO. I am enclosing a request to publish this document on the internet. I would like to publish the Auxiliary Lagrangian Drifter Dataset on the internet as well; in order to further this idea, and to explore some other ideas I have with the Navy, I would like to attend the "6.4 Transitions" meeting which will be held the last week of January at the Stennis Space Center. Peter Niiler will be giving a talk and will discuss some of the work which I have done at this meeting.

I am looking forward to meeting you in San Diego at your earliest convenience.

I'd be glad to answer any questions you might have. For your convenience: (619) 753-9328; spazan@cts.com. The E-mail address is different from that Harry Selsor used to contact me (spazan@aol.com). I'm shifting the burden of my E-mail to the cts site, partly because of the heavy traffic on America OnLine which you may have read about recently.

Sincerely yours,
Stephen Pazan
Stephen Pazan